https://doi.org/10.1016/j.jcsr.2021.106696 This is the Pre-Published Version.

Structural response of high strength S690 welded sections under cyclic loading conditions

[a,b]Ho H.C., [b]Guo Y.B., [a,b]Xiao M., [a]Xiao T.Y., [a,b]Jin H., [a,c]Yam M.C.H., [a,b]Chung K.F.[*], and [d]Elghazouli A.Y.

[a] Chinese National Engineering Research Centre for Steel Construction (Hong Kong Branch), The Hong Kong Polytechnic University, Hong Kong SAR, PR China.
[b] Department of Civil and Environmental Engineering, The Hong Kong Polytechnic University, Hong Kong SAR, PR China.
[c] Department of Buildings and Real Estate, The Hong Kong Polytechnic University, Hong Kong SAR, PR China.
[d] Department of Civil and Environmental Engineering, Imperial College London, U.K.

Corresponding author: kwok-fai.chung@polyu.edu.hk

Abstract

High strength S690 steel offers an attractive solution for use in buildings and bridges, owing to the inherent high strength to self-weight ratio of the material which can lead to significant savings in terms of cost and time. However, take up in practice has been hampered by concerns related to the deterioration in mechanical properties of the S690 steel plates after welding as a result of changes in microstructure. Whilst recent studies have illustrated the high levels of ductility that can be provided by the S690 steel, it is essential to assess and quantify the inelastic cyclic response of welded sections made from the same material. This paper therefore presents an experimental investigation into the structural response of high strength S690 welded sections under various cyclic loading conditions. A detailed description of 32 cyclic tests, carried out under two different cyclic protocols with various combinations of target strains and loading frequencies, is provided. Particular focus is given to examining the strength degradation in the material, the number of effective cycles completed before fracture, and the energy dissipation performance. A direct comparsion is also provided between the cumulative cyclic response of the S690 welded sections and their unwelded S690 plate counterparts, based on which the detrioration in behaviour is readily quantified. It is shown that a significant deterioration in strength similarly occurs in both the unwelded and welded S690 sections with the increase in number of cycles, particularly under large target strains. However, in terms of ductility, the number of effective cycles to fracture of the S690 welded sections are found to be considerably lower than for the S690 steel plates, typically by a factor of 2 to 3. Moreover, the energy dissipation densities of the S690 welded sections are shown to be only 41% to 47% of those for the counterparts. Overall, in addition to highlighting the importance of conducting realistic cyclic tests for assessing ductility, the findings provide detailed insights into the structural response of the S690 welded steel sections, including the influence of target strains and loading frequencies. The results also enable detailed quantification of the cyclic response for the purpose of numerical modelling as well as for determining reliable ductility criteria.

Keywords:

High strength steel; Welded sections; Cyclic loading; Hysteretic behaviour; Ductility.

1. Introduction

High strength steels have been examined extensively over the past two decades because of their highly favourable strength to self-weight ratios which enable the development of improved structural systems and the use of more efficient construction methods. In recent years, high strength steels have been employed in heavily loaded members of large lifting equipment in mines, port facilities and offshore platforms. In the presence of potential adverse effects of welding on the microstructures of high strength steels, there have been some concerns with respect to their applicability in seismic resistant structures [1]. This is due to the possible deterioration in the mechanical properties of their welded sections, particularly in terms of strength and ductility which are of vital importance for seismic resistances.

Welding is a common process in steelwork fabrication, which is required to be carried out by skilled welders with highly specialized equipment and specific procedures. All structural steelwork should be inspected after fabrication to ensure that there is no defect present in the weldments. In general, common structural steels, such as S235 and S355 steels, are *ferritic* or *ferritic-pearlitic* steels, and there is no significant change in their microstructures after welding. Hence, it is widely accepted that welded sections from such steels are typically not prone to any reduction in mechanical properties, unlike in high strength steel materials.

High strength steels are commonly produced with carefully controlled heat-treatments [2], such as *Quenching-and-Tempering* for QT steels, and *Thermal-Mechanically-Controlled-Process* for TM steels, in order to attain specific martensitic-ferritic microstructures which possess favourable mechanical properties. These high strength steels, such as S690-QT and S690-TM, have been readily produced in many modern steel mills around the world for the past twenty years. However, microstructural changes in heat-affected-zones (HAZ) of welded S690 plates could be triggered during welding if not performed properly. Once the maximum temperature, T_{max}, at the fusion line of the welded sections, exceeds certain threshold values during welding [2], significant phase changes, re-crystallization and grain growth, take place (Fig. 1). Various phases including *martensite, bainite, ferrite* and *pearlite* of different volumetric fractions are then formed according to their specific cooling times from 800 ^{o}C to 500 ^{o}C, within a time $t_{8/5}$ (Fig. 2) under practical air cooling conditions after welding. It should be noted that the whole process of microstructural changes in the HAZ of S690 welded sections depends primarily on the welding procedures and parameters, particularly the heat input energy, q (kJ/mm), during welding, the plate thicknesses as well as the joint details. Since the behaviour of such S690 welded sections depends heavily on the mechanical properties of the HAZ, it is essential to control the welding procedures and parameters in order to minimize deteriorations in the strength and ductility of S690 welded sections [3].

A number of previous investigations [4, 5, 6] were conducted to examine the microstructural changes in S690 welded sections. Similar studies into co-relating the mechanical properties of various HAZ to those of S690 welded sections using high-fidelity micro-mechanical models and meso-scale mechanical analyses were also reported [7, 8]. Many of these investigations examined SEM images and volumetric fractions of the HAZ as well as their strengths and hardness as a means of assessing their physical and mechanical properties. However, limited attention has been given to assess the ductility of such materials for structural applications under cyclic loadings. There is, therefore, a pressing need to undertake focused structural evaluations of the response of S690 welded sections subjected to large inelastic deformations under various cyclic loading conditions.

1.1 Strength and ductility requirements for high strength S690 steels

Modern codes of practice stipulate a number of ductility requirements for structural steels. For example, EN 1993-1-1 [9] and EN 1993-1-12 [10] require the following:

a) for S235 to S460 steels:

i) $f_u / f_y \geq 1.10$; ii) $\varepsilon_L \geq 15\%$; and iii) $\varepsilon_u \geq 15\,\varepsilon_y$ (1a)

b) for high strength steels up to S700:

i) $f_u / f_y \geq 1.05$; ii) $\varepsilon_L \geq 10\%$; and iii) $\varepsilon_u \geq 15\,\varepsilon_y$ (1b)

where ε_y , ε_u , and ε_L are the strains corresponding to the yield strength, f_y, the tensile strength, f_u, and fracture of the steel matrerial.

The above requirements have been formulated based on standard tensile tests on steel coupons under monotonic actions, first develped about 75 years ago and updated regularly over many years. These standard tensile tests are relatively simple and from which engineering stress-strain curves are readily obtained to provide key mechanical properties. Besides, they have been conducted for many years in material laboratories of steel mills as a mean of quality control on their production.

In recent years, a number of experimental investigations [11, 12, 13] have shown that the mechanical properties of common structural steels, such as S235 and S355, as well as the higher strength S690 steels, are significantly different under monotonic and cyclic actions. However, whilst the reliability of welded S355 steel sections have been examined, information is lacking on the strength and ductility characteristics of S690 welded sections under inelastic cyclic loading conditions. At present, it is not known whether the ductility requirements given in Eqn.(1) are adequate for structures, incorporating S690 steel materials, and subjected cyclic seismic actions. Currently, no specific requirements for the structural response of S690 steels and their welded sections are stipulated in structural design codes. There is also an absence of detailed guidance [9, 10, 14] on assessing the structural behaviour of welded sections and joints employing high strength S690 steels under cyclic loadings. Hence, this lack of systematic experimental assessments and technical guidance prohibit an effective use of high strength S690 steels in seismic resistant structures in many parts of the world.

1.2 Previous work on the cyclic response of high strength steels

Numerous experimental investigations into both the strength and the ductility properties of structural steels and metal alloys under cyclic actions have been reported in the literature over the past forty years. These studies can be classified into two main categories:

a) For the vibration assessment in the serviceability limit state, high-cycle low-strain cyclic tests were commonly employed to investigate the long term fatigue behaviour of welded sections in steel structures as well as various types of metal alloys in aircrafts and automobiles [15, 16, 17, 18]. Typical numbers of cycles in such tests ranged from 0.5 to 50 million, while the stress levels were typically between 5 to 30 % of the yield strengths of the steels or the metal alloys.

b) For structures subjected to seismic actions, either simulated quasi-static cyclic tests or shaking table tests were employed to examine the response of structures. For members or connections, a number of cyclic protocols with various low-cycle high-strain cyclic loadings [19, 20, 21 & 22] were considered to be appropriate.

A preliminary experimental investigation into the strength and the ductility properties of S690 steel plates (un-welded) under cyclic actions was previously conducted by the authors [12]. A total of 36 funnel-shaped coupons, with a diameter of 5.0 mm at mid-length, were tested as follows:

a) A cyclic protocol with non-linearly increasing strains according to FEMA 461 [23] was adopted, in which the strain magnitude ε was multiplied by an amplification factor of 1.4 after every two cycles. The test was considered to be successfully completed when the coupon was able to attain the specified target strain, ε_T, at both the 19^{th} and 20^{th} cycles.

b) These cyclic tests were carried out for four target strains, ε_T of ±2.5%, ±5.0%, ±7.5% and ±10.0%, and also for four loading frequencies, f_L of 0.1, 0.5, 1.0 and 2.0 Hz. The magnitudes of both the target strains ε_T and loading frequencies f_L were selected according to typical seismic response in buildings and bridges.

It should be noted that for each combination of target strain ε_T and loading frequency f_L, two coupons were tested to allow comparison of the test data in order to assess the repeatability of the test results. It was found that:

- All 36 coupons of the S690 steels exhibited effective hysteretic behaviour under various combinations of the target strains ε_T and loading frequencies f_L.

- Only 28 out of the 36 coupons were able to complete the tests successfully, i.e. to attain the target strains ε_T at ±2.5%, ±5.0% and ±7.5% under loading frequencies f_L of 0.1, 0.5, 1.0 and 2.0 Hz at both the 19^{th} and 20^{th} cycles. However, fracture occurred in the other 8 coupons after completion of only the 19^{th} cycle when the target strains ε_T were increased to ±10.0%, irrespective of the loading frequency f_L.

- In general, the effect of loading frequency f_L within the range of 0.1 and 2.0 Hz on the cyclic behaviour of S690 steels was shown to be relatively insignificant.

It has therefore been readily concluded that S690 steels possessed a high degree of ductility under such cyclic actions. As it has long been accepted that S355 steels exhibits good ductility under monotonic tensile actions, it was important to assess the structural response of S690 steels under cyclic actions compared to those of S355 steels. Such an experimental

investigation was hence conducted recently by the authors [13], where a total of 32 funnel-shaped coupons were tested under two different cyclic protocols with combinations of four target strains ε_T and two loading frequencies, f_L. In addition to the cyclic protocol with non-linearly increasing strains according to FEMA 461 as mentioned above, a cyclic protocol with constant strains throughout a test was also introduced. It was found that:

- For tests carried out under the cyclic protocol of non-linearly increasing strains, similar structural response was obtained for both S355 and S690 steels under the same combinations of target strains ε_T , and loading frequencies, f_L .

- For tests conducted under the cyclic protocol of constant strains, the response of S355 and S690 steels varied considerably according to the magnitudes of the target strains. For ε_T = ±2.5%, and f_L of 0.1 and 1.0 Hz, S690 steels were unable to complete the same numbers of cycles as the S355 steels. When ε_T was increased to ±5.0%, ±7.5% and ±10%, with f_L of 0.1 and 1.0 Hz, the total numbers of cycles completed in the cyclic tests of both S355 and S690 steels were significantly reduced, as expected. However, S690 steels were *unexpectedly* found to be able to complete more cycles than S355 steels in all these cases, demonstrating a superior cyclic deformation characteristic under such large target strains.

There is, however, a need to extend the above evaluations into S690 welded sections and to assess their structural response in comparison with that of un-welded S690 steels under various cyclic conditions. This is essential in order to quantify the strength and ductility of welded S690 steels with a view to examine their applicability in seismic design.

1.3 Objectives and scope of work

In order to promote effective engineering applications of high strength S690 steels in heavily loaded structural members in buildings and bridges, it is essential to achieve efficient and robust structural performance under various loading conditions. More specifically, both the S690 steel members and their joints are required to achieve reliable strength and ductility properties under both monotonic and cyclic loadings. This paper presents a detailed experimental investigation into the structural response of welded sections from high strength S690 steels. The study aims to quantify their structural response under two different cyclic protocols with various combinations of target strains and loading frequencies. The primary objective of the experimental investigation is to assess the applicability of S690 steels in seismic applications, and to quantify any degradation in the structural response of welded sections under various cyclic loadings, when compared with those of un-welded counterparts.

The experimental investigation comprises the following series of tests:

a) Standard tensile tests

   Standard tensile tests are conducted on two coupons of S690 steel plates as well as two coupons of S690 welded sections. The load-elongation curves of these four coupons are

obtained to give basic mechanical properties of these coupons under monotonic tension as reference data for subsequent assessments.

b) Cyclic axial tension and compression tests

Cyclic axial tests are conducted on 16 coupons of S690 steel plates as well as 16 coupons of S690 welded sections, under cyclic tension and compression actions according to two carefully controlled cyclic protocols:

- Cyclic Protocol NL where the strains increase progressively in a non-linear manner up to a total of 20 cycles according to FEMA 461 [23] (Fig.3a), where the target strain, ε_T, is the strain at the 19th and the 20th cycles; and

- Cyclic Protocol CT where the strains in all cycles are kept equal to the target strain, ε_T, up to fracture (Fig. 3b).

Through a detailed test programme, various load-deformation curves of these coupons are obtained to compare and contrast their cyclic response under four different target strains, ε_T, and two different loading frequencies, f_L. Moreover, images of Scanning Electronic Microscopy (SEM) on selected coupons of both S690 steel plates and welded sections are obtained to illustrate their typical microstructures.

The chemical compositions of S690 steels, stipulated in EN 10025: Part 6 [24] according to the delivery condition of quenching and tempering, are summarized in Table 1a). All the monotonic and cyclic tests were conducted with a high precision Instron 8803 Servo Hydraulic Fatigue Testing System with a capacity of 500 kN. Key areas of interest of the present experimental investigation are:

i) degradation in both the strength and ductility of S690 welded sections, when compared with those of S690 un-welded steel plates;
ii) ability of these coupons to undergo large cyclic deformations as defined by the number of effective cycles completed before fracture, n_c, under various cyclic actions;
iii) energy dissipation densities of the S690 welded sections, and
iv) typical microstructures in the HAZ of the S690 welded sections.

All the funnel-shaped coupons are standard coupons specially devised for cyclic axial tension and compression tests in which the coupons may be required to deform up to a strain of 10 to 15% under compression without buckling. However, based on previous experience [12, 13, 15, 19], these coupons may still buckle at their mid-lengths under large compressive strains, depending on the testing equipment and attachment, as well as the material specifications and geometrical dimensions of the coupons.

1.4 Robotic welding

In order to achieve highly consistent welding quality in the S690 welded sections, a robotic welding system was employed to carry out welding (Fig. 4a) for the present investigation according to various established practice on welding procedures and parameters. The chemical compositions of the electrode adopted in this investigation are also presented in Table 1b),

while all the key parameters for robotic welding are summarized in Table 2. It should be noted that a total of 5 weld runs were adopted in the welding so that the heat input energy of each weld run is controlled within the range of 0.96 to 1.06 ± 0.02 kJ/mm.

Cutting and machining details used in preparing the test coupons of both the steel plates and the welded sections are also illustrated in Fig. 4b). It should be noted that all funnel-shaped coupons of the welded sections were carefully machined using a numerical control machine so that the fusion line of the heat-affected-zones are located precisely at the mid-length of their gauge lengths, i.e. the critical cross-sections with minimum cross-sectional areas. Detailed dimensions of all the coupons are also illustrated in Fig. 4c).

A detailed account of the experimental arrangements and test results for the axial cyclic tests as well as the complementary standard tensile tests is provided below. This is followed by comparative and quantitative assessments of the degradation in strength, ductility and energy dissipation in welded S690 plates subjected to various cyclic loading conditions.

2. Standard Tensile Tests

In order to compare the load-elongation curves of coupons from the S690 steel plates and the S690 welded counterparts, a total of four standard tensile tests were conducted in accordance with BS EN ISO 6892-1 [25]. The test programme is summarized in Table 3a) while the test set-up is illustrated in Fig. 5. As it is important to obtain precise "stress and strain" conditions of the coupons during tests, an extensometer with an accuracy of 0.0015 mm was used to measure the elongation of the coupons over a gauge length of 10.00 ±0.01 mm. In addition, a non-contact method of precision measurement, referred to as Digital Photos Analysis, is employed in which a large number of images of the deformed coupons are captured and recorded with the use of a digital video camera throughout the tests. Owing to the high resolution of about 24 million pixels per image, instantaneous dimensions of the coupons with an accuracy at ±0.0125 mm are readily obtained after data analyses.

Based on the measured dimensions of the coupons, the engineering stress-strain (σ_e - ε_e) curves of all the coupons for both the S690 steel plates and the S690 welded sections were obtained from the measured applied loads and the measured elongations. These curves are plotted onto the same graph (Fig. 6) for direct comparison, while key results of the tests are summarized in Table 3b). It is shown that the stress-strain curves of both the S690 steel plates and the S690 welded sections follow closely one another, not only in the initial yielding stages but also in the large deformation stages towards fracture. It is evident that softening occurs in the S690 welded sections just before yielding, when compared with that of the S690 steel plates. Moreover, the average elongation at fracture, ε_L, of the S690 welded sections is around 20.0 % on average, which is lower than that of the S690 steel plates at 23.8 %.

Typical fractured coupons are illustrated in Fig. 7, together with enlarged views of the fractured surfaces. It is apparent from the figure that failure, in the form of tension fracture, is initiated at the centre of the coupons, followed by a shear fracture in the rest of the cross-section of the coupon.

3. Cyclic Axial Tension and Compression Tests

A total of 16 coupons of the S690 welded sections were carefully prepared according to the dimensions shown in Fig. 4c). These coupons were tested under both Cyclic Protocols NL and CT (Fig.3) with various combinations of four different target strains ε_T , i.e. ε_T = ±2.5%, ±5.0%, ±7.5% and ±10.0%, and two different loading frequencies f_L, i.e. f_L = 0.1 and 1.0 Hz. Similarly, another 16 coupons of the S690 steel plate counterparts were also prepared and tested to provide reference data for direct comparison. Table 4 summarizes the test programme of the cyclic tests, and the typical experimental set-up is shown in Fig. 5.

Based on the measured dimensions of the coupons, the measured applied loads, as well as the measured axial elongations and shortenings of the coupons under various cyclic actions, the engineering stress-strain (σ_e - ε_e) curves are obtained. These curves are plotted onto graphs

which are presented in a consistentc manner for direct comparison of the structural response for various target strains, and subsequently for various loading frequenices. Comparisons between these graphs are described below.

3.1 Engineering stress-strain (σ_e - ε_e) curves under Cyclic Protocol NL

All the engineering stress-strain (σ_e - ε_e) curves of both the S690 steel plates and the S690 welded sections are shown (Figs. 8 and 9) to be effective hysteretic loops with significant energy dissipation characteristics under Cyclic Protocol NL. It is evident that the structural response of both the S690 steel plates and the S690 welded sections under these cyclic actions are similar, even with the loading frequencies f_L differing by a factor of 10 in the two figures.

The numbers of effective cycles of the coupons completed before fracture, n_c, under Cyclic Protocol NL with various combinations of target strains ε_T and loading frequencies f_L are presented in Table 5. It should be noted that as there is a level of softening in some of the curves, an effective cycle is defined as a hysteretic loop in which the strength of the coupon at a specific target strain does not deteriorate below 75% of its orginial value.

Comparison among the graphs in Figs. 8 and 9, as well as the values of n_c in Table 5, reveals the following:

a) For cyclic tests with ε_T = ±2.5%, ±5.0% and ±7.5%, for f_L = 0.1 and 1.0 Hz

- Almost all the coupons from both the S690 steel plates and the S690 welded sections completed the tests successfully, i.e. they were able to complete the 20th cycle without fracture. Hence, the number of effective cycles completed before fracture, n_c, for these coupons is 20.

  The only exception is, however, the coupon of S690 welded sections which fractured after completion of the 19th cycle under a target strain ε_T of ±7.5% and f_L = 0.1, and hence, n_c is 19 for this coupon.

- There was no sign of softening in the engineering stress-strain (σ_e - ε_e) curves as they overlap one another very well along the full range of deformations, and hence, there is no evidence of deterioration in their structural response under these cyclic actions.

b) For cyclic tests with ε_T = ±10.0 %, for f_L = 0.1 and 1.0 Hz

- As the target strain ε_T was increased to ±10.0 %, all the coupons of the S690 steel plates fractured after completion of only the 19th cycle of the tests. Owing to the presence of the HAZ in the coupons of S690 welded sections, their performance was inferior to those of the S690 steel plates. Hence, the values for n_c of both the S690 steel plates and the S690 welded sections are as follows:
  - 19 and 16, respectively when f_L = 0.1 Hz, and
  - 19 and 17, respectively when f_L = 1.0 Hz.

It should be noted that although the values of n_c only differ by a maximum of 3 out of 20 in these cases, their maximum strains achieved in these cyclic tests differ by a factor of 1.4 x 1.4 (i.e. 1.96).

- There was no sign of softening in the engineering stress-strain (σ_e - ε_e) curves as they overlap one another very well along the full range of deformations, and hence, there is no evidence of deterioration in their structural response under these cyclic actions.

3.2 Engineering stress-strain (σ_e - ε_e) curves under Cyclic Protocol CT

All the engineering stress-strain (σ_e - ε_e) curves for both the S690 steel plates and the S690 welded sections are shown (Figs. 10 and 11) to be effective hysteretic loops with significant energy dissipation characteristics under Cyclic Protocol CT. It is evident that the response of both the S690 steel plates and the S690 welded sections under these cyclic actions are similar, even with the loading frequencies f_L differing by a factor of 10 in the two figures.

The number of effective cycles of the coupons completed before fracture, n_c, under Cyclic Protocol CT with various target strains ε_T and loading frequencies f_L are also presented in Table 5. Comparison among the graphs in Figs. 10 and 11 as well as the values of n_c in Table 5 reveals that:

a) For cyclic tests with ε_T = ±2.5% and ±5.0%, or f_L = 0.1 and 1.0 Hz

- The values of n_c for the S690 steel plates and the S690 welded sections with ε_T =±2.5% are:

  - 58 and 18, respectively, for f_L = 0.1 Hz, and
  - 54 and 21, respectively, for f_L = 1.0 Hz.

- The values of n_c for the S690 steel plates and the S690 welded sections with ε_T at ±5.0% are:
  - 16 and 8, respectively, for f_L = 0.1 Hz, and
  - 17 and 8, respectively, for f_L = 1.0 Hz.

- There is an apparent deterioration in strength and ductility for the S690 welded sections as shown in their hysteretic loops, when compared with those of the S690 steel plates. Degradation in their structural response is evident under large accumulated cyclic deformations.

b) For cyclic tests with ε_T = ±7.5% and ±10.0%, for f_L = 0.1 and 1.0 Hz

- Under these target strains, the S690 steel plates and the S690 welded sections exhibit relatively ineffective cyclic response, irrespective of the loading frequency.

- The values of n_c for the S690 steel plates and the S690 welded sections for $\varepsilon_T = \pm 7.5\%$ are:
  - 8 and 4, respectively, for $f_L = 0.1$ Hz, and
  - 9 and 4, respectively for $f_L = 1.0$ Hz.

- The values of n_c for the S690 steel plates and the S690 welded sections for $\varepsilon_T = \pm 10.0\%$ are:
  - 6 and 1, respectively, for $f_L = 0.1$ Hz, and
  - 5 and 2, respectively, for $f_L = 1.0$ Hz.

- Significant deterioration in both the strength and the ductility of the S690 welded sections are shown in the hysteretic loops; the degradation in structural response is also evident under larger accumulated cyclic deformations.

In general, it is shown that the number of cycles to fracture, n_c , of the S690 welded sections is typically smaller than that of the S690 steel plates by a factor of 2 to 3. Hence, Cyclic Protocol CT is evidently more demanding, when compared with Cyclic Protocol NL, in differentiating between the structural response of S690 welded sections and that of S690 steel plates under severe cyclic actions.

Fig. 12 illustrates typical fractured coupons after testing together with enlarged views of the fractured surfaces. It should be noted that the ripples that appear on the fractured surfaces of these coupons under cyclic actions are very different from those in the standard tensile tests (Fig. 7).

3.3 Microstructure of fractured coupons

A detailed investigation into the microstructures of the fractured coupons of both the S690 steel plates and the S690 welded sections was undertaken. After careful machining and polishing, an optical microscope with a magnification power of 2,000 times was employed to examine the entire fractured coupons. A Scanning Electron Microscope with a magnification power of 500,000 times was also employed to examine the microstructures of specific locations of the coupons. The main observations are summarised as follows:

a) As shown in Fig. 13, a highly consistent homogeneous microstructure of the tempered martensite is present throughout the gauge length of a typical coupon of the S690 steel plate, and fracture occurs at the cross-section with the minimum area, as expected.

b) In contrast, for a typical welded coupon, Fig. 14 reveals a microstructure which is very different from that shown in Fig. 13. It shows a heterogeneous microstructure with significant variations in grain sizes along the longitudinal direction due to the effects of welding. In the vicinity of the fusion line, three different forms of microstructures having various phases are readily identified as follows:

   i) Type HAZ-HT with long lath martensite,

ii) Type HAZ-MT with short lath martensite, and
iii) Type HAZ-LT with a dual phase of martensite and ferrite.

It should be noted that such a heterogeneous microstructure is the result of the practical (uncontrolled) air cooling process after welding in which phase change, re-crystallization and grain growth into various phases of the steels take place according to their cooling rates $t_{8/5}$. As the strength of the microstructure in Type HAZ-LT is known to be weaker than those of the other two types, fracture takes place within Type HAZ-LT, as expected.

In general, formation of Type HAZ-LT in the S690 steel plates after welding depends on many factors, such as: i) chemical compositions and heat treatment, ii) welding procedures and parameters (including plate thickness, joint details, numbers of weld passes, welding equipment, and hence, heat input energy in each pass), and iii) cooling rate $t_{8/5}$. Owing to the change in microstructure of the S690 steel plates, the mechanical properties of the S690 welded sections may be very different from those of the S690 steel plates. Further detailed information on these aspects can be found elsewhere [2, 4, 12].

4. Comparative Assessment of Cyclic Deterioration

This section provides more detailed quantification of the structural response of the S690 welded sections under various cyclic actions, with a focus on assessing the deterioration in key response parameters in comparison with those of the S690 un-welded counterparts.

4.1 Deterioration in strength

In order to quantify the deterioration in strength of the S690 welded sections under Cyclic Protocol CT with various cyclic actions, Figs. 10 and 11 are re-plotted in Fig 15. In the latter, only the first and the last cycles in each of the cyclic tests are shown in the same graphs. Hence, the extent of deterioration in the strength of the coupons is readily illustrated. Similarly, the deterioration in the strength of the coupons from un-welded S690 steel plates are also plotted and presented in the figure for direct comparison. Moreover, two strength modification factors, η_t and η_c , are established to quantify strength degradation of both the S690 steel plates and the S690 welded sections, which are defined as follows:

$$\eta_t = f_{\varepsilon T,t} / f_y \quad (2a)$$

$$\eta_c = f_{\varepsilon T,c} / f_y \quad (2b)$$

where $f_{\varepsilon T,t}$ is the strength at a target (tensile) strain, $+\varepsilon_T$, under cyclic action,

$f_{\varepsilon T,c}$ is the strength at a target (compressive) strain, $-\varepsilon_T$, under cyclic action, and

f_y is the yield strength, i.e. the 0.2% proof strength, in the engineering stress-strain curve obtained in a standard tensile test.

All the strength modification factors, η_t and η_c , of the S690 welded sections under a specific target strain ε_T and a specific loading frequency f_L under Cyclic Protocl CT are plotted onto the same graphs. Similar graphs are also prepared for the S690 steel plates. All of these graphs for cyclic tests under various target strains ε_T , i.e. ε_T = ±2.5%, ±5.0%, ±7.5% and ±10.0%, and loading frequencies f_L , i.e. f_L = 0.1 and 1.0 Hz, are presented in Fig. 16. In order to facilitate direct comparison, Table 6 summarizes the values of both the strength modification factors η_t and η_c of both the S690 steel plates and the S690 welded sections at the first cycle under various target strains and loading frequencies.

It can be observed that:

a) As shown in Table 6 for the case with a loading frequency f_L = 0.1 Hz, when the target strains increase from ±2.5% to ±10.0%:

i) the values of η_t of the steel plates at the first cycle decrease from 1.03 to 0.94 while the corresponding values of η_c increase from 1.15 to 1.33, and
ii) the values of η_t of the welded sections at the first cycle decrease from 1.11 to 1.01 while the corresponding values of η_c increase from 1.29 to 1.47.

Moreover, the values of η_t and η_c of the welded sections at the first cycle are always larger than those of the welded sections. Similar results are also obtained for the other case with a loading frequency f_L = 1.0 Hz.

b) As shown in Figure 16, there is always a significant deterioration in the strengths of both the S690 steel plates and the S690 welded sections with decreasing values of η_t and η_c after accumulated cyclic deformations in all cyclic tests. Hence, the values of both η_t and η_c tend to decrease in a non-linear manner when the cycle numbers increase, and such reductions are more pronounced under large target strains.

4.2 Deterioration in ductility

In order to conduct a systematic comparison between various engineering stress-strain curves, the normalized engineering stress ratio β_e is adopted, which is given by:

$$\beta_e = \sigma_e / f_y \qquad 3)$$

where σ_e is the engineering stress measured in the cyclic test, and

f_y is the yield strength, i.e. the 0.2% proof strength, in the engineering stress-strain curve obtained in a standard tensile test.

All the engineering stress-strain (σ_e - ε_e) curves in Figs. 8 to 11 were modified into normalized engineering stress ratio-engineering strain (β_e - ε_e) curves, for the different target strains ε_T and loading frequency f_L to enable direct comparison. This is discussed below as follows:

a) Hysteretic loops under Cyclic Protocol NL

- Fig. 17 plots all the envelopes of the normalized engineering stress ratio - engineering strain (β_e - ε_e) curves of the S690 steel plates and the S690 welded sections. It is evident that the extent of cyclic softening among these coupons under different target strains is insignificant.

- The backbone curves from the cyclic tests of both the S690 steel plates and the S690 welded sections are derived according to the recommendations of the NEHRP Seismic Design Brief 2010 [26], and the Guidelines for Performance-Based Seismic Design for Tall Buildings [27]; these curves are also plotted in Fig. 17.

- The engineering stress-strain (σ_e - ε_e) curves of the S690 steel plates and the S690 welded sections obtained from the standard tensile tests (Fig.6) are also plotted in Fig.17, normalized with respect to f_y. This allows a comparison of the structural response of the S690 steel plates and the S690 welded sections under monotonic and cyclic actions to be readily made.

b) Hysteretic loops under Cyclic Protocol CT

- Fig. 18 plots all the normalized engineering stress ratio – engineering strain (β_e - ε_e) curves of the S690 steel plates and the S690 welded sections. The extent of cyclic softening can be readily compared. It is apparent that deterioration in the ductility of these coupons under different target strains are very significant.

- The values of n_c for both the S690 steel plates and the S690 welded sections are also provided in Fig. 18 to facilitate the comparison. Hence, the deterioration in the ductility of both the S690 steel plates and the S690 welded sections under various cyclic actions are fully illustrated. As stated in Section 3.2, the number of effective cycles to fracture, n_c , of the S690 welded sections is typically smaller than that of the S690 steel plates by a factor of 2 to 3.

- Even though the hysteretic loops of both the S690 steel plates and the S690 welded sections are very similar in shapes and sizes, the S690 welded sections are shown to be inferior to the S690 steel plates owing to a significant reduction in the values of n_c .

- The engineering stress-strain (σ_e - ε_e) curves of the S690 steel plates and the S690 welded sections obtained from the standard tensile tests (Fig. 6) are also plotted in Fig. 18, normalized with respect to f_y. This allows a comparison of the response of the S690 steel plates and the S690 welded sections under monotonic and cyclic actions to be readily made.

4.3 Deterioration in energy dissipation densities

The energy dissipation performance of the coupons is readily quantified in term of the energy dissipated per unit volume of steel, referred to herein as the energy dissipation density. The energy dissipation densities of the coupons of the S690 steel plates and the S690 welded sections under various monotonic and cyclic actions are evaluated and discussed as follows:

a) Standard tensile tests

The energy dissipation density of the coupons of either the S690 steel plates or the S690 welded sections, E_{SP} and E_{WS}, respectively, under monotonic tension is readily evaluated according to the area enclosed within an engineering stress-strain (σ_e - ε_e) curve. It is evident that the S690 welded sections exhibit lower levels of elongation at fracture of 20.0% or less on average, when compared with 23.8% for the S690 steel plates (Fig.6).

The average energy dissipation densities for both the S690 steel plates and the S690 welded sections, E_{SP} / E_{WS}, were determined to be 303 and 234 MJ/m^3, and hence, the value of the ratio E_{WS} / E_{SP} was found to be 0.77.

b) Cyclic axial tension / compression tests under Cyclic Protocol CT

The energy dissipation density of the S690 steel plates or the S690 welded sections, e_i, per cycle can be readily evaluated from the area enclosed within the engineering stress-strain (σ_e - ε_e) curve for each cycle [23, 24]. After detailed data analyses, the energy dissipation density for each of the cycles of both the S690 steel plates and the S690 welded sections, e_{sp} and e_{ws} , under various combinations of target strains ε_T and loading frequencies f_L, were obtained. These are plotted in Fig. 19 to illustrate their variations, and hence, their energy dissipation performance throughout the cyclic tests. It is evident that these curves follow broadly the variations of deterioration in the strength of both the S690 steel plates and the S690 welded sections, as illustrated in the strength modification factors of the cyclic tests shown in Fig. 16.

After summing up the values of e_{sp} and e_{ws} for the entire tests under various target strains and loading frequencies, the corresponding total energy dissipation densities E_{SP} and E_{WS} of both the S690 steel plates and the S690 welded sections are plotted in Fig. 20. The values of both E_{SP} and E_{WS} for all the cyclic tests with various combinations of target strains ε_T and loading frequencies f_L are also presented in Table 7.

It is evident from the results that the values of E_{SP} are significantly larger than their E_{WS} counterparts under all combinations of target strains ε_T and loading frequencies f_L. The ratios of E_{WD} / E_{SP} under various target strains ε_T differ significantly as they range from 0.19 to 0.54 with an average value of 0.41 for f_L = 0.1 Hz. Similarly, these ratios range from 0.43 to 0.53 with an average value of 0.47 for f_L = 1.0 Hz. Hence, it is clearly shown that the S690 welded sections provide less favourable response compared to that of the S690 steel plates under Cyclic Protocol CT due to the significant deterioration in their energy dissipation densities.

5. Conclusions

This paper presented a detailed experimental investigation into structural response of high strength S690 welded sections under various cyclic loading conditions. A total of 32 cyclic tests were carried out under two different cyclic protocols with various combinations of target strains ε_T and loading frequencies f_L. Particular focus was given to assessing key structural response related to the cyclic tests, including: i) strength deteriorations, ii) numbers of effective cycles completed before fracture, and iii) energy dissipation densities. The main structural repsonse parameters for the S690 welded sections subjected to cumulative cyclic loading were quantified and compared with those of the unwelded S690 steel plate counterparts. A number of important conclusions can be drawn from this study:

a) In general, Cyclic Protocol CT, in which constant strain amplitude cycles are applied up to fracture, is significantly more demanding when compared with the more gradual Cyclic Protocol NL. Whilst the former is considered an overly severe representation of seismic loading, it can be used as an effective approach for assessing the inelastic cyclic response of the S690 welded sections in comparison with that of the S690 steel plates.

b) Cyclic softening in the hysteretic loops of the coupons of the S690 welded sections under Cyclic Protocol CT were evident. The corresponding numbers of cycles completed before fracture, n_c, for the S690 welded sections were found to be typically only half or even one third of those for the S690 steels. Hence, the structural response of the S690 steel plates was shown to deteriorate more significantly after welding under various cyclic actions.

c) Deteriorations in both the strength and energy dissipation performance of the S690 welded sections under accumulated cyclic deformations according to Cyclic Protocol CT were more severe than those of the S690 steel plates. These deteroriations were readily quantitied in terms of the numbers of effective cycles completed before fracture, the strength modification ratios and the energy dissipation densities.

The test results showed that there is always a significant deterioration in the strengths of both the S690 steel plates and the S690 welded sections when the cycle numbers increase, with such reductions being more pronounced under large target strains. In terms of ductility, the number of effective cycles to fracture, n_c, for the S690 welded sections were shown to be considerably lower than that for the S690 steel plates, typically by a factor of 2 to 3. Moreover, the energy dissipation densities of the S690 welded sections, E_{WS} , were found to be only 0.41 to 0.47 of those of the S690 steel plates, E_{SP}.

Overall, the experimental assessments and discussions presented in this study provide detailed insights into the structural response of S690 welded sections under various cyclic loading conditions, and emphasize the importance of going beyond monotonic tensile tests in quantifying ductility. The results also provide novel experimental data that can be used in calibrating detailed numerical cyclic models, as well as offer quantified information that can be used for determining ductility criteria for use in assessment and design procedures.

ACKNOWLEDGEMENT

This investigation is part of a large research project entitled "Effective Use of High Strength Steels in Construction" of the Chinese National Engineering Research Centre for Steel Construction (Hong Kong Branch) at the Hong Kong Polytechnic University. The CNERC is funded by the Innovation and Technology Fund of the Innovation and Technology Commission of the Government of the Hong Kong SAR, and the Research Committee of the Hong Kong Polytechnic University (Project Nos. 1-BBY3, BBY6 & BBV3). The research work is also partially funded by the Research Grants Council of the University Grants Committee of the Government of Hong Kong SAR (Project Nos.: 152687/16E, 152231/17E and 157152/18E). Financial support for various research studies (Project Nos. RJKB) from the Research Committee of the Hong Kong Polytechnic University is gratefully acknowledged.

Robotic welding was performed in the Welding Laboratory of the Industrial Centre while all axial tests on steel coupons under monotonic and cyclic actions were conducted at the Building Technology Laboratory at the Hong Kong Polytechnic University. Technical support from the technicians is gratefully acknowledged.

REFERENCES

1. Willms R. (2009). High strength steel for steel construction. Proceedings of Nordic Steel Construction Conference, 597-604.
2. Easterling KE. (1992). Introduction to Physical Metallurgy of Welding, Butterworth - Heinemann.
3. Ho HC, Chung KF, Huang MX, Nethercot DA, Liu X, Jin H, Wang GD and Tian ZH. (2020). Mechanical properties of high strength S690 steel welded sections through tensile tests on heat-treated coupons. Journal of Construction Steel Research, 166: 105922.
4. Mayr P. (2007). Evolution of microstructure and mechanical properties of the heat affected zone in B-containing 9% chromium steels. Ph.D. Thesis. Faculty of Mechanical Engineering, Graz University of Technology, Austria.
5. Ding Q, Wang T, Shi Z, Wang Q, Wang Q, and Zhang F. (2017). Effect of welding heat input on the microstructure and toughness in simulated CGHAZ of 800 MPa Grade steel for hydropower penstocks. Metals; 7(4):115.
6. Azhari F, Al-Amin Hossain A, Heidarpour A, Zhao XL, and Hutchinson CR. (2018). Mechanical response of ultra-high strength (Grade 1200) steel under extreme cooling conditions. Constructional Building Materials; 175:790–803.
7. Śloderbach Z. and Pająk J. (2015). Determination of ranges of components of heat affected zone including changes of structures. Archives of metallurgy and materials, 60(4): 2607-2612.

8. Tian Y, Wang HT, Li Y, Wang ZD and Wang GD. (2017). The analysis of the microstructure and mechanical properties of low carbon micro-alloyed steels after ultra-fast cooling. Materials Research, 20(3): 853-589.
9. CEN (2005). EN-1993-1-1:2005, Eurocode 3: Design of Steel Structures – Part 1-1: General rules and rules for buildings. European Committee for Standardization, Brussels, Belgium.
10. CEN (2007). EN 1993-1-12:2007, Eurocode 3: Design of Steel Structures – Part 1-12: Additional rules for the extension of EN 1993 up to steel grades S700. European Committee for Standardization, Brussels, Belgium.
11. Wang YB, Li GQ, Sun X, Chen SW and Hai LT (2017). Evaluation and prediction of cyclic response of Q690D steel. Proceedings of the Institution of Civil Engineers - Structures and Buildings 170 (11): 788-803.
12. Ho HC, Liu X, Chung KF, Elghazouli AY, and Xiao M. (2018). Hysteretic behaviour of high strength S690 steel materials under low cycle high strain tests. Engineering Structures 165: 222-236.
13. Guo YB, Ho HC, Chung KF, and Elghazouli AY. (2020). Cyclic deformation characteristics of S355 and S690 steels under different loading protocols. Engineering Structures 221: 111093.
14. AISC (2016). ANSI/AISC 360-16: Specification for Structural Steel Buildings. American Institute of Steel Construction, Chicago, U.S.A.
15. Fournier B, Sauzay M, Caës C, Noblecourt M, and Mottot M. (2006). Analysis of the hysteresis loops of a martensitic steel – Part I: Study of the influence of strain amplitude and temperature under pure fatigue loadings using an enhanced stress partitioning method. Material Science and Engineering: A, 437: 183-196.
16. Fournier B, Sauzay M, Caës C, Mottot M and Noblecourt M, and Pineau A. (2006). Analysis of the hysteresis loops of a martensitic steel – Part II: Study of the influence of creep and stress relaxation holding times on cyclic behaviour. Material Science and Engineering: A, 437: 197-211.
17. Khan S, Wilde F, Beckmann F and Mosler J. (2012). Low cycle fatigue mechanism of the lightweight alloy Al2024. International Journal of Fatigue, 38: 92-99.
18. Chen Y, Sun W and Chan TM. (2013). Effect of loading protocols on the hysteresis behaviour of hot-rolled structural steel with yield strength up to 420 MPa. Advanced Structural Engineering, 16 (4): 707-719.
19. Nip KH, Gardner L, Davies CM, and Elghazouli AY. (2010). Extremely low cycle fatigue tests on structural carbon steel and stainless steel. Journal of Constructional Steel Research, 66: 96-110.
20. Zhou F, Chen Y and Wu Q. (2015). Dependence of the cyclic response of structural steel on loading history under large inelastic strains. Journal of Constructional Steel Research, 104: 64-73.
21. Wang YB, Li GQ, Cui W, Chen SW and Sun FF. (2015). Experimental investigation and modelling of cyclic behaviour of high strength steel. Journal of Constructional Steel Research, 104: 37-48.
22. Hu F and Shi G. (2018). Constitutive model for full-range cyclic behaviour of high strength steel without yield plateau. Constructional Building Materials, 162: 596-607.
23. FEMA-461. (2007). Interim testing protocols for determining the seismic performance characteristics of structural and nonstructural components. Washington D.C., U.S.A. Federal Emergency Management Agency, Department of Homeland Security.

24. BS EN 10025-6 (2019). Hot rolled products of structural steels. Technical delivery conditions for flat products of high yield strength structural steels in the quenched and tempered condition, British Standards Institution.

25. BS EN ISO 6892-1. (2009). Metallic materials – Tensile testing: Part 1: Method of test at ambient temperature, British Standards Institution.

26. Deierlein G, Reinhorn A and Willford M. (2010). NEHRP Seismic Design Technical Brief No. 4 - Nonlinear Structural Analysis for Seismic Design: A Guide for Practicing Engineers, NIST.

27. Guidelines for Performance-Based Seismic Design for Tall Buildings (2017). Pacific Earthquake Engineering Centre (PEER), Report No. 2017/06.

POctB19

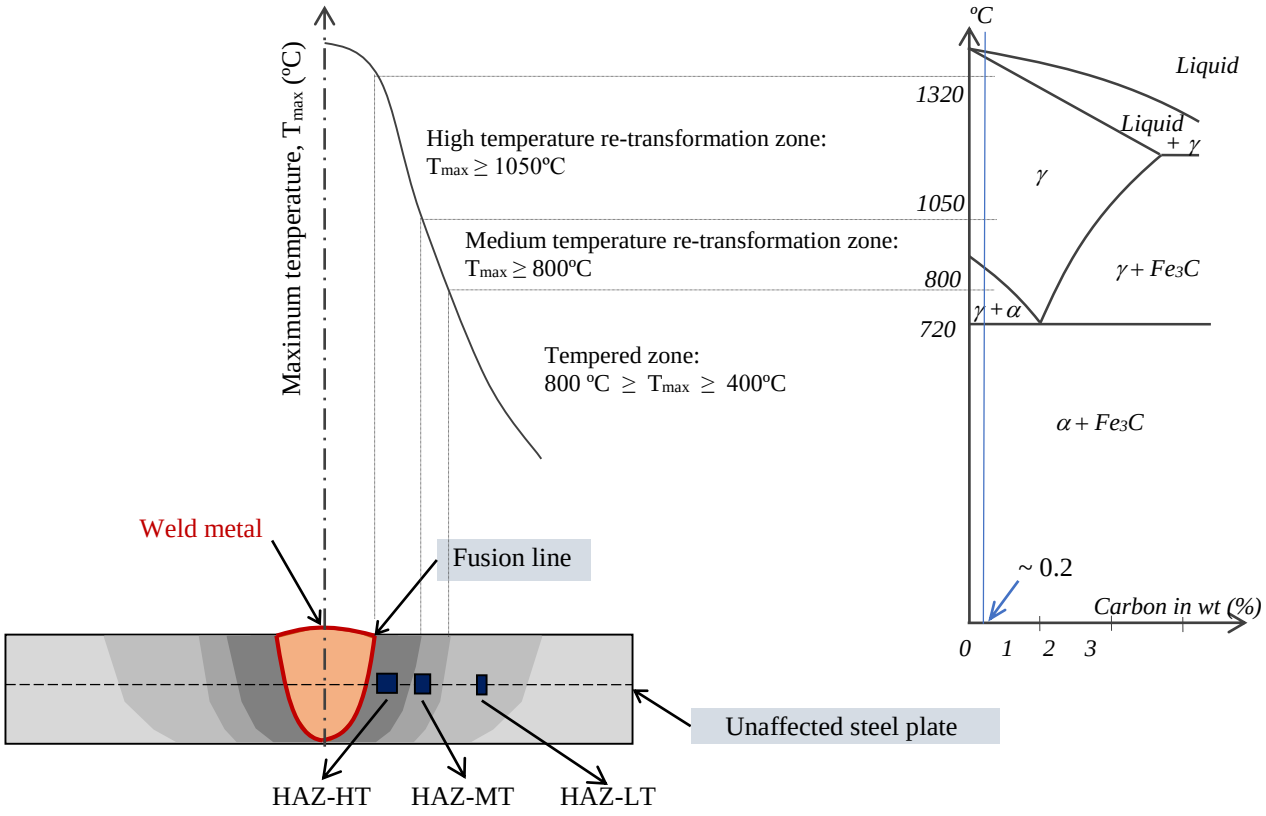

Figure 1 Heat-affected zones in S690 welded sections after a single pass welding

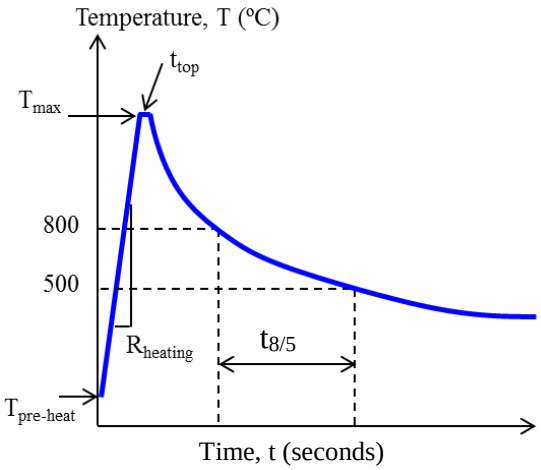

Figure 2 Temperature history at specific positions of a welded section

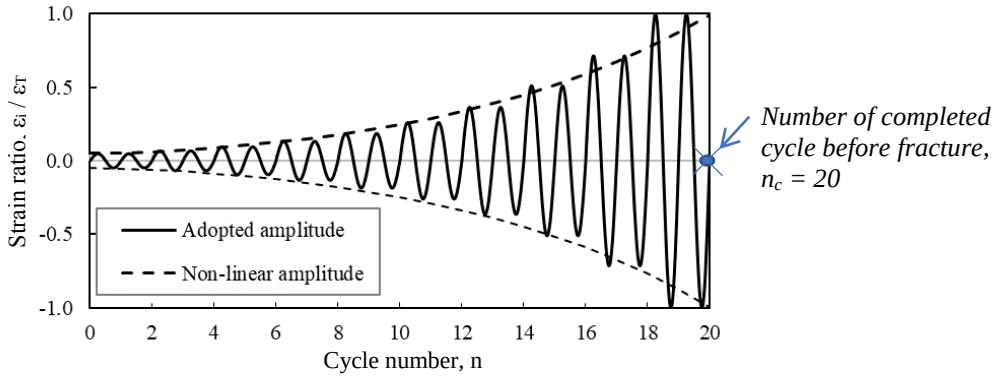

a) Cyclic Protocol NL
The strain increases non-linearly.

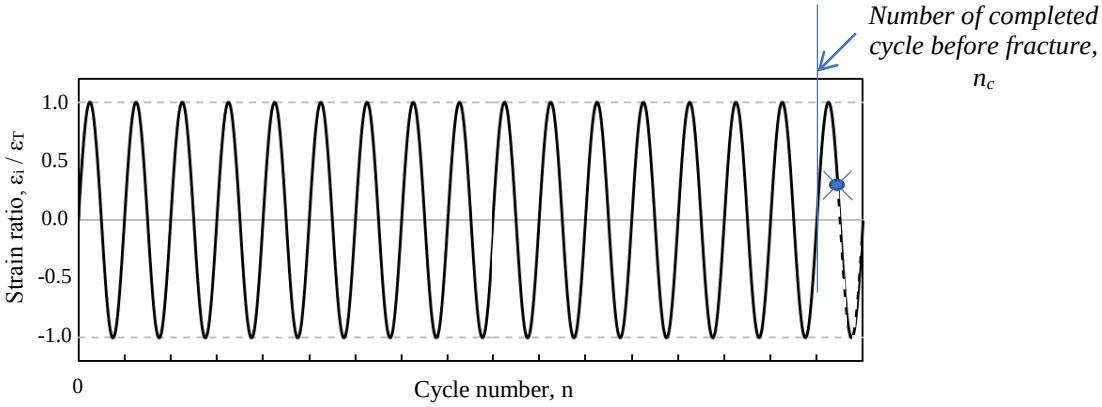

b) Cyclic Protocol CT
The strain is constant.

Figure 3 Cyclic Protocols NL and CT

a) In-house robotic welding using a Fanuc-i100 Welding Robot by GMAW

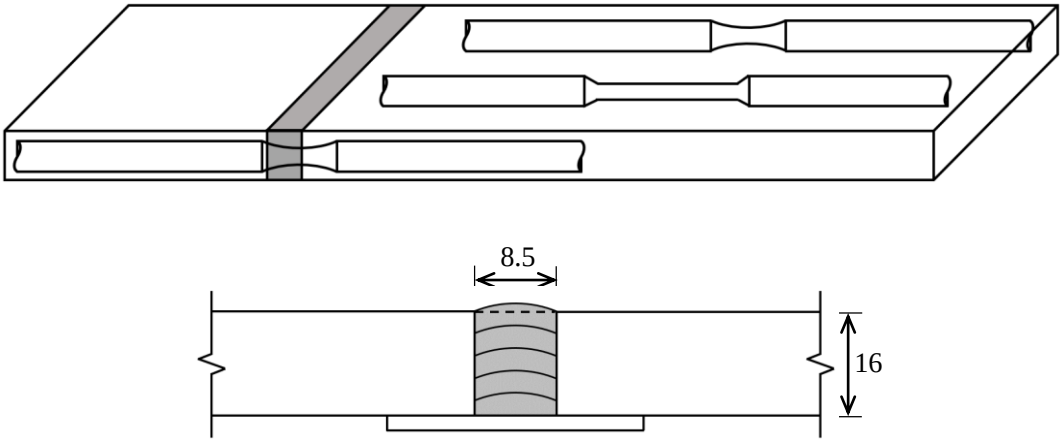

b) Welding of steel plates, and details of welding joints

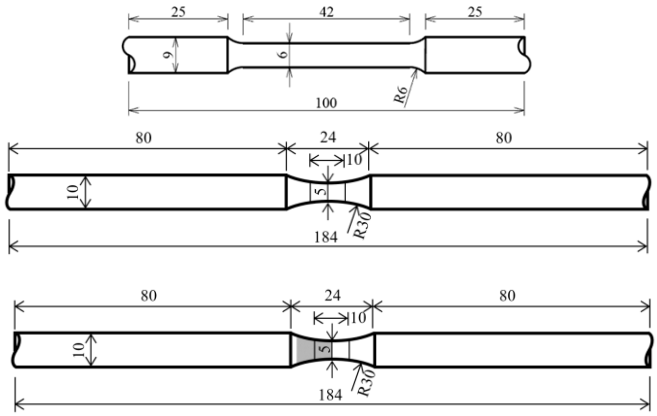

c) Dimensions of test coupons

Figure 4 Robotic welding and preparation of test coupons of S690 steel plates and welded sections

Figure 5 Test set-up for both monotonic and cyclic tests

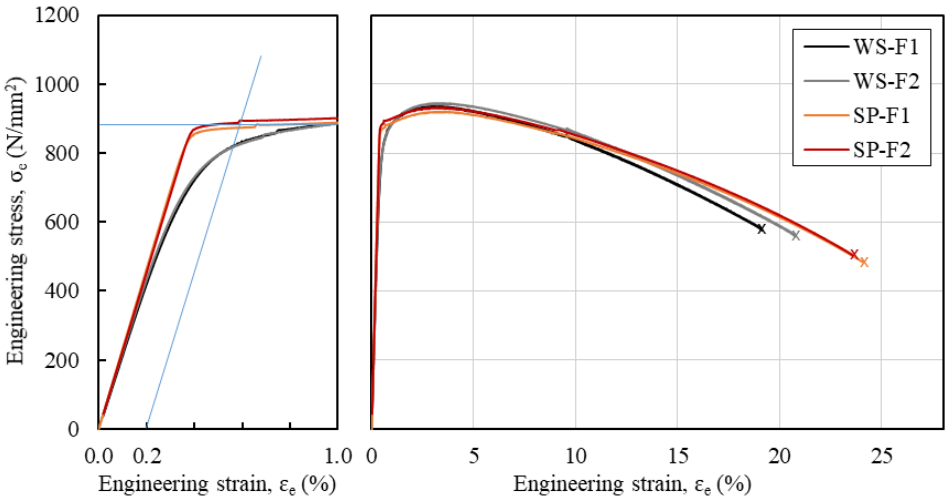

Figure 6 Measured engineering stress-strain curves of funnel-shaped coupons under standard tensile tests

a) Typical funnel-shaped coupon before testing

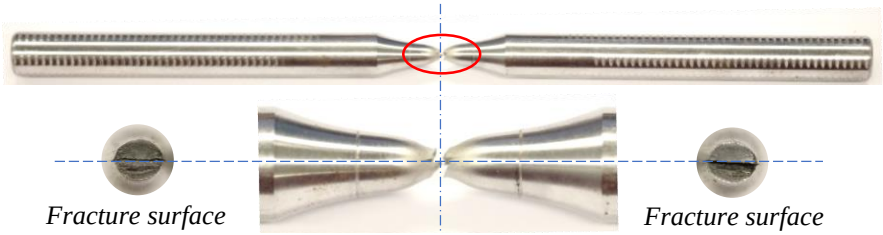

b) Typical fractured coupon of the S690 steel plate after test

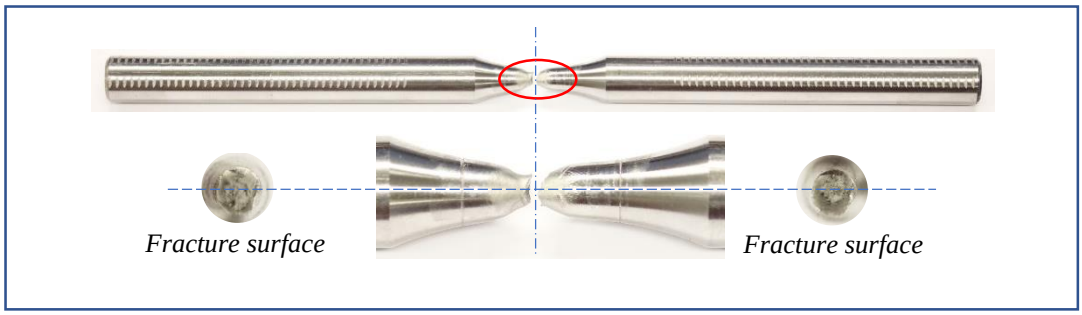

c) Typical fractured coupon of the S690 welded section after test

Figure 7 Funnel-shaped coupons under standard tensile tests

Loading frequency, f_L = 0.1 Hz

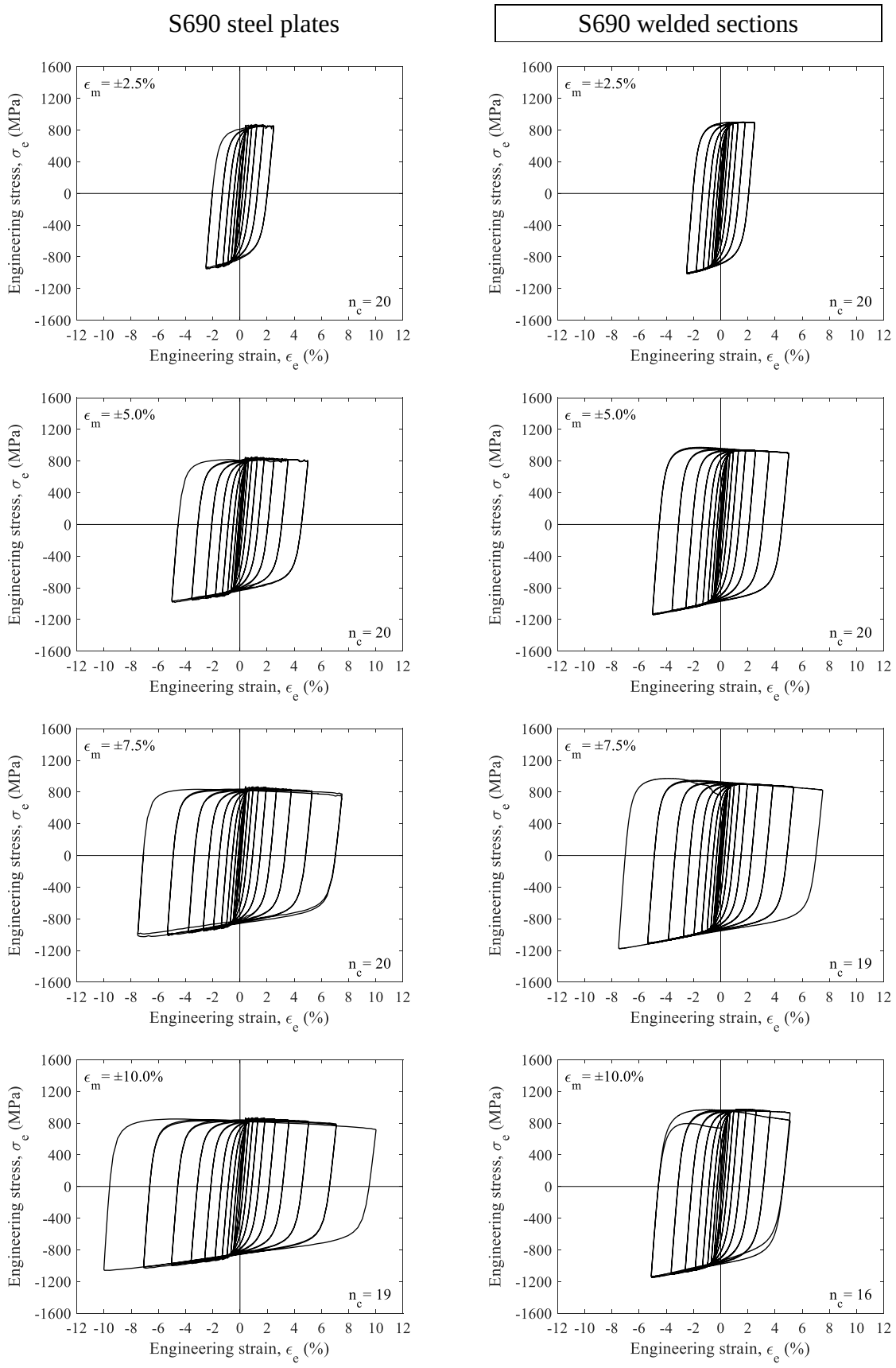

Figure 8 Engineering stress-strain (σ_e - ε_e) curves under Cyclic Protocol NL with f_L = 0.1 Hz

Loading frequency, f_L = 1.0 Hz

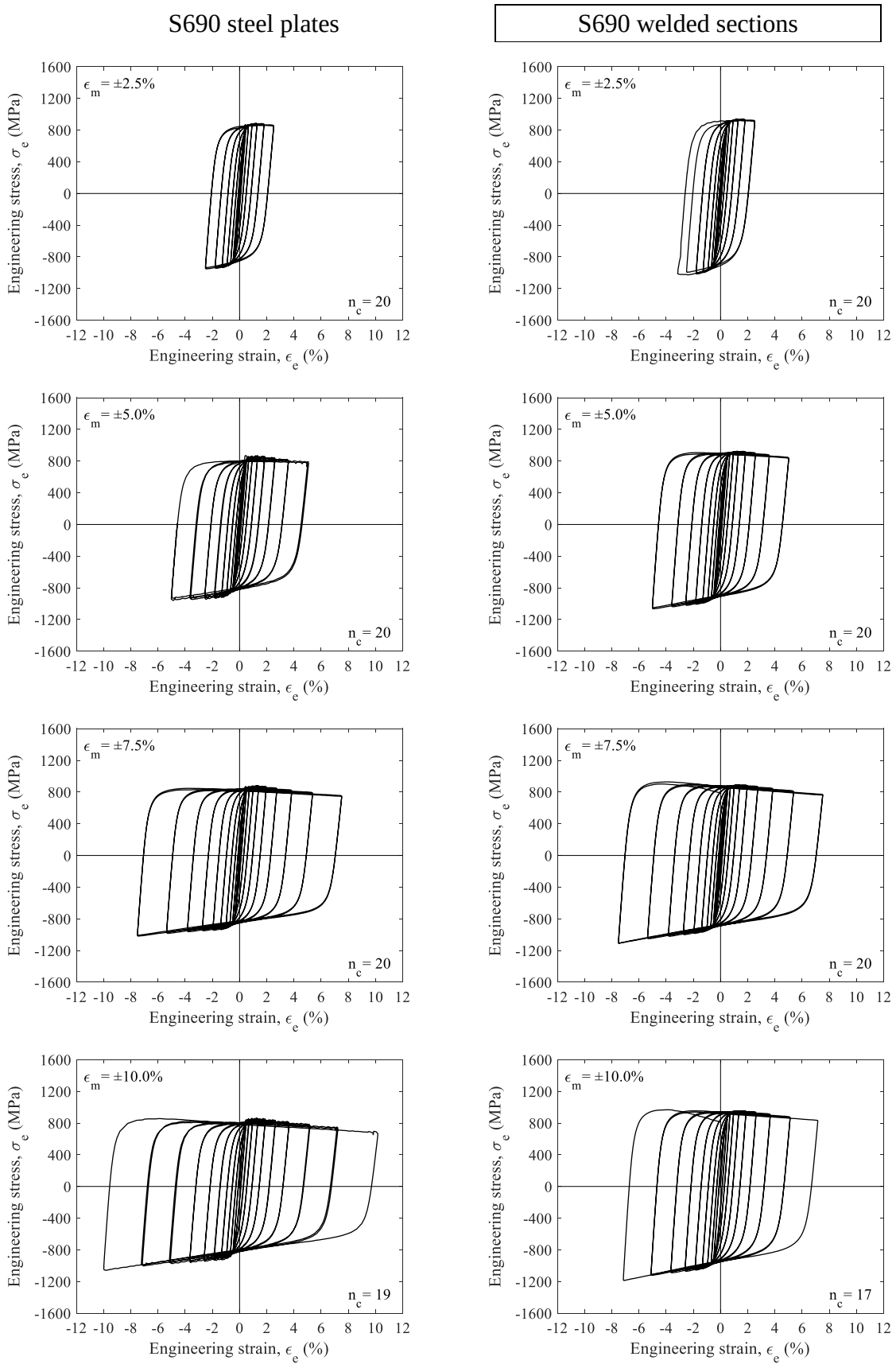

Figure 9 Engineering stress-strain (σ_e - ε_e) curves under Cyclic Protocol NL with f_L = 1.0 Hz.

Loading frequency, f_L = 0.1 Hz

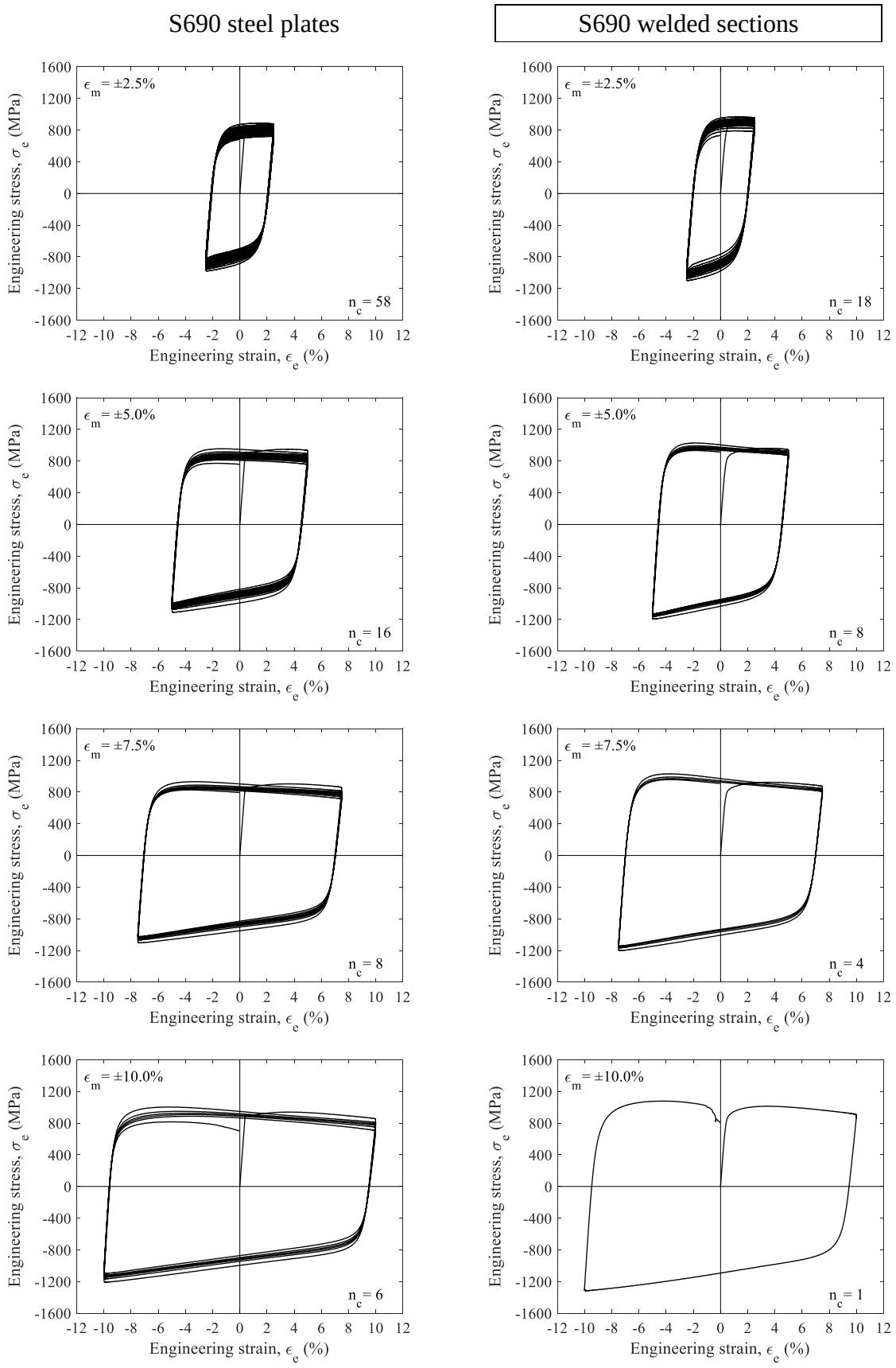

Figure 10 Engineering stress-strain (σ_e - ε_e) curves under Cyclic Protocol CT with f_L = 0.1 Hz

Loading frequency, f_L = 1.0 Hz

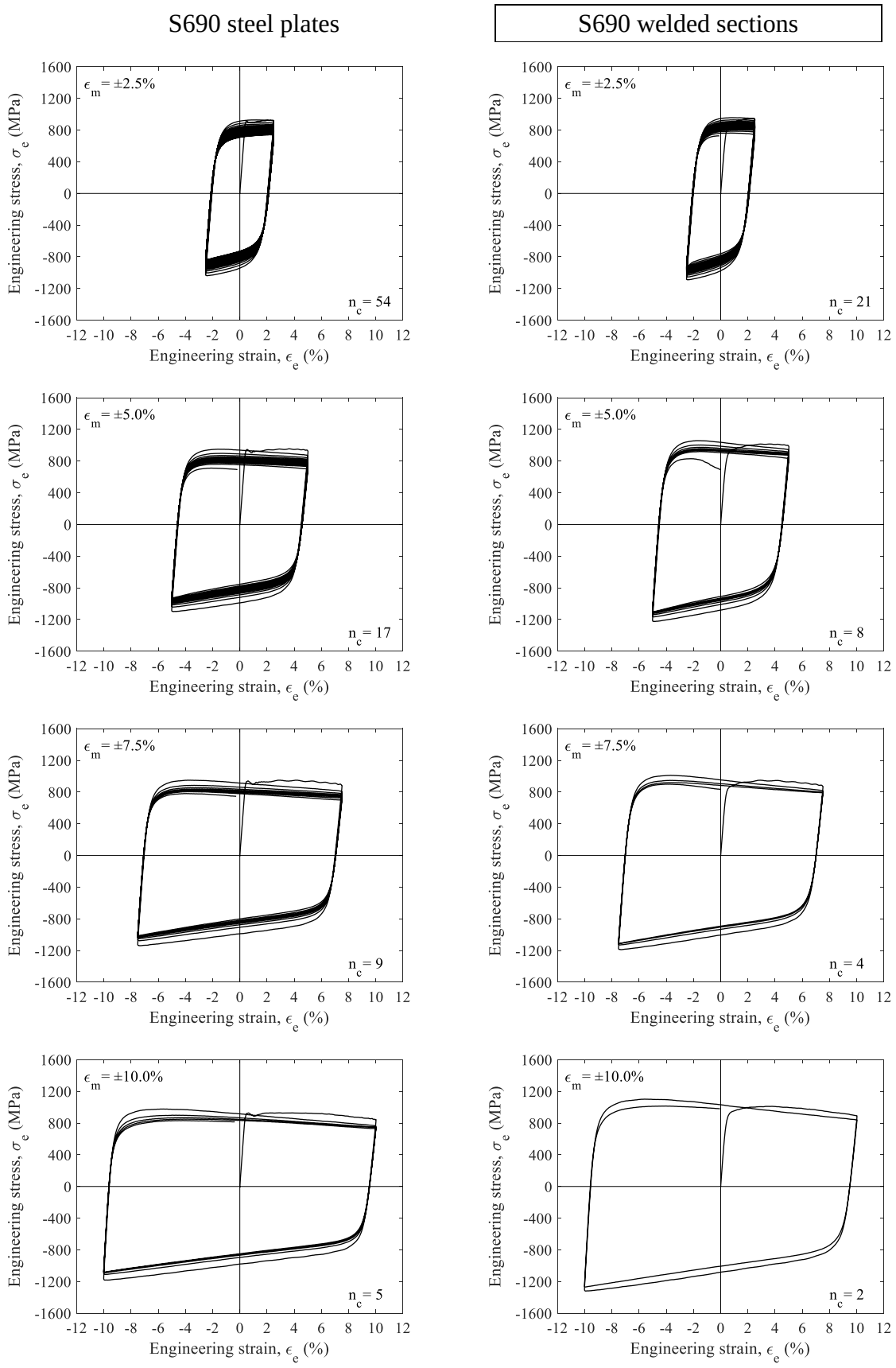

Figure 11 Engineering stress-strain (σ_e - ε_e) curves under Cyclic Protocol CT with f_L = 1.0 Hz.

a) Typical funnel-shaped coupon before testing

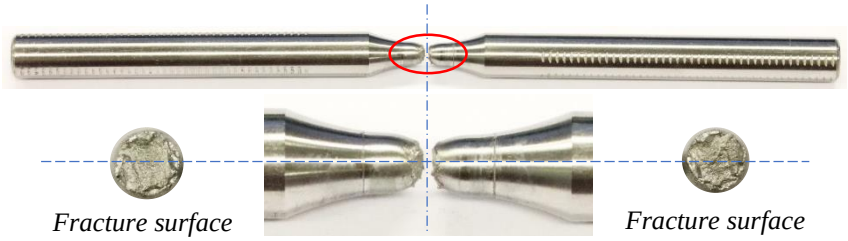

b) Typical fractured coupon of the S690 steel plate after test

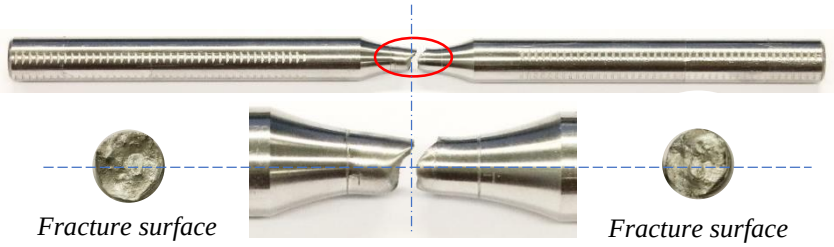

c) Typical fractured coupon of the S690 welded section after test

Figure 12 Funnel-shaped coupons under cyclic tests

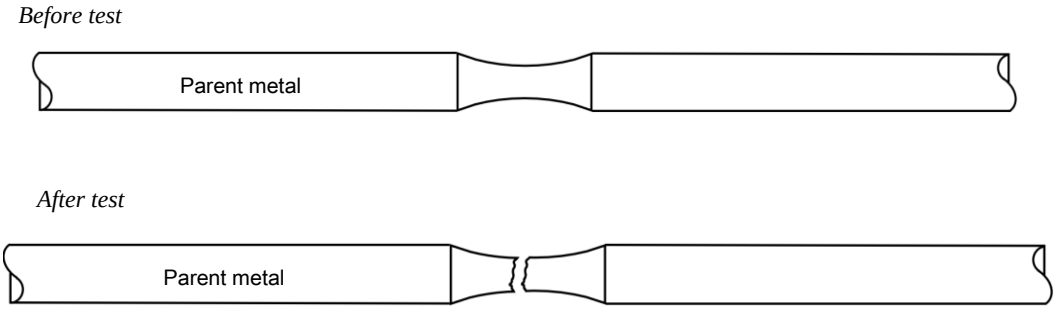

a) Macroscopic view of a test coupon of S690 steel plate

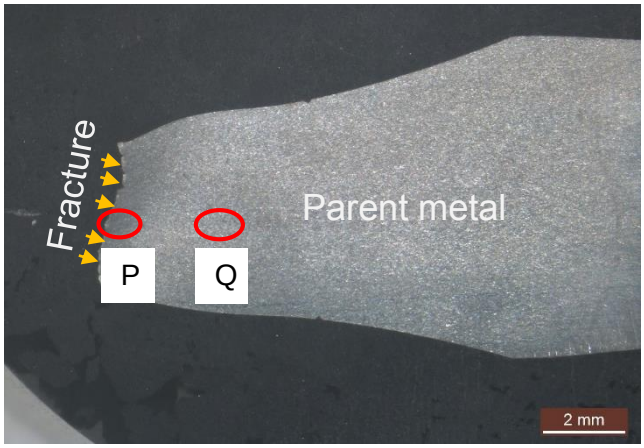

b) Optical images of a fractured coupon

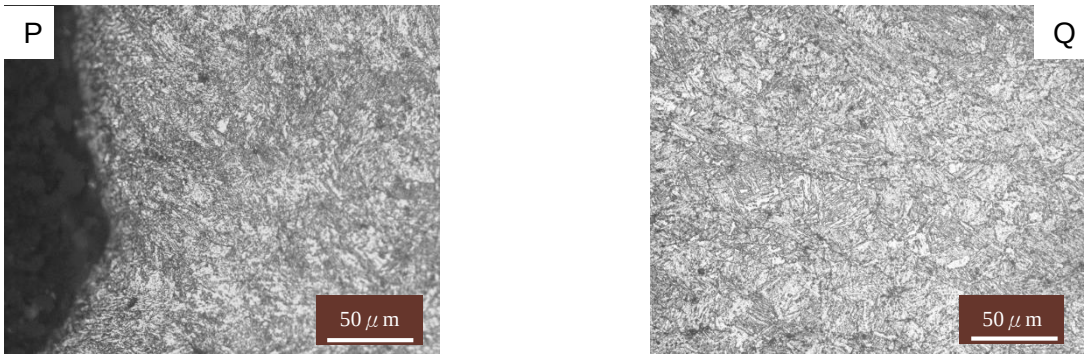

Tempered martensite Tempered martensite

c) Microscopic images of a fractured coupon

Figure 13 Macroscopic and microscopic views of a typical fractured coupon of the S690 steel plate

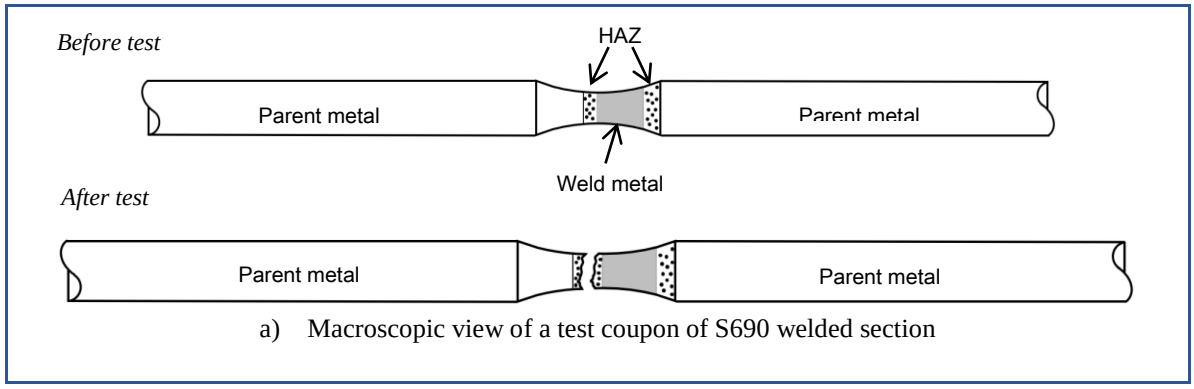

a) Macroscopic view of a test coupon of S690 welded section

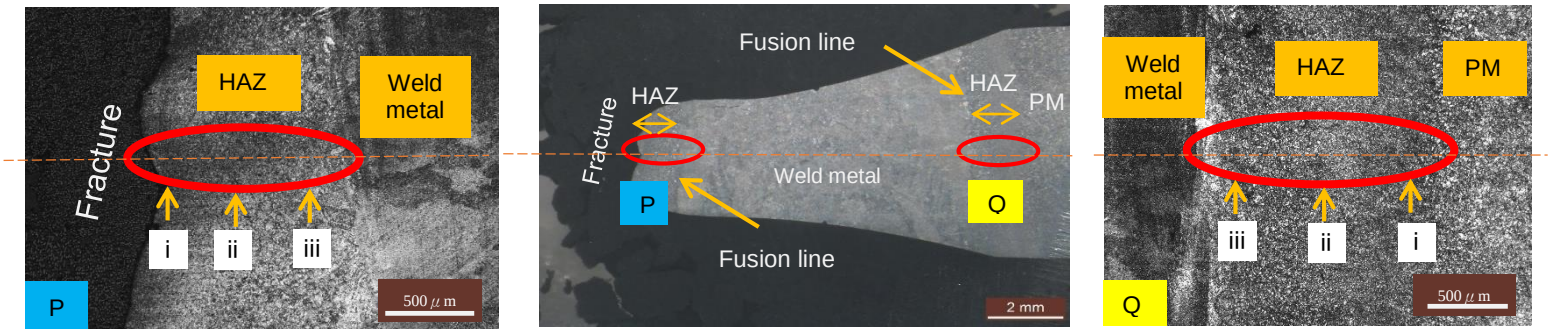

b) Optical images of a fractured coupon

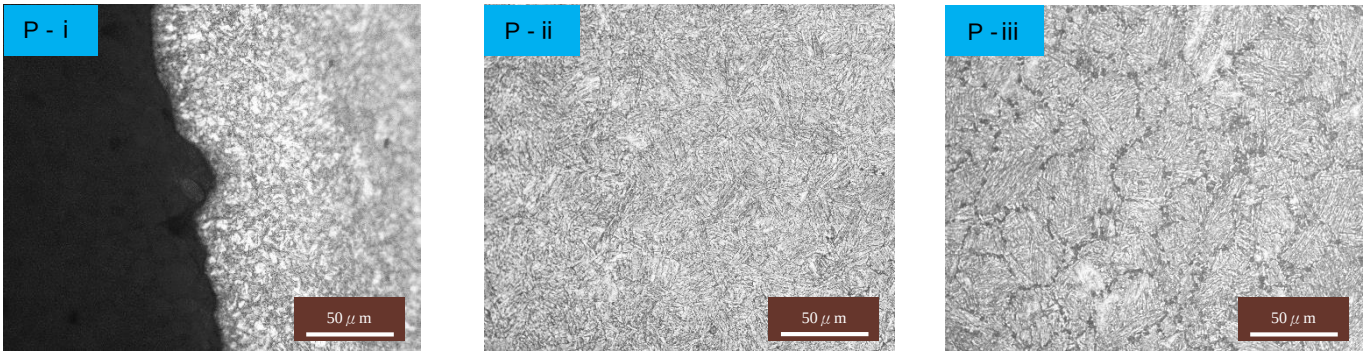

HAZ-LT with dual phase martensite and ferrite | HAZ-MT with short lath martensite | HAZ-HT with long lath martensite

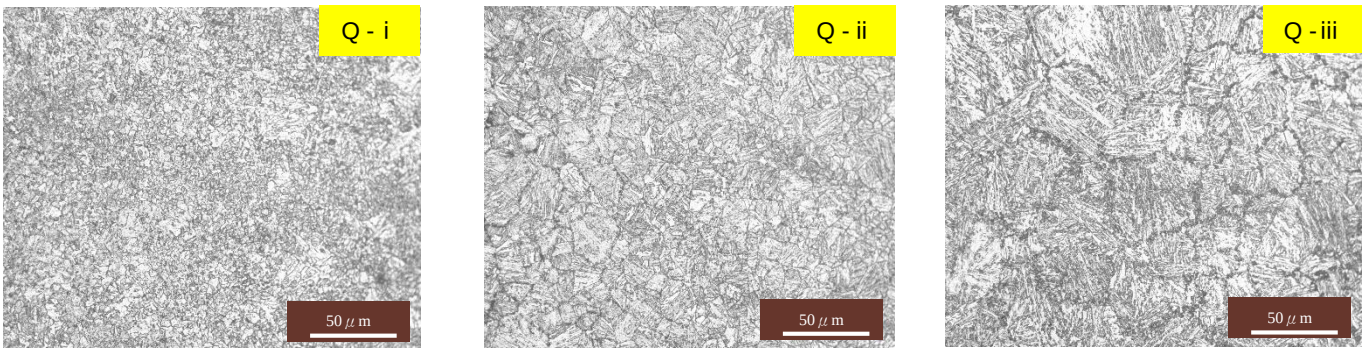

HAZ-LT with dual phase martensite and ferrite | HAZ-MT with short lath martensite | HAZ-HT with long lath martensite

c) Microscopic images of a fractured coupon

Figure 14 Macroscopic and microscopic views of a typical fractured coupon of the S690 welded section

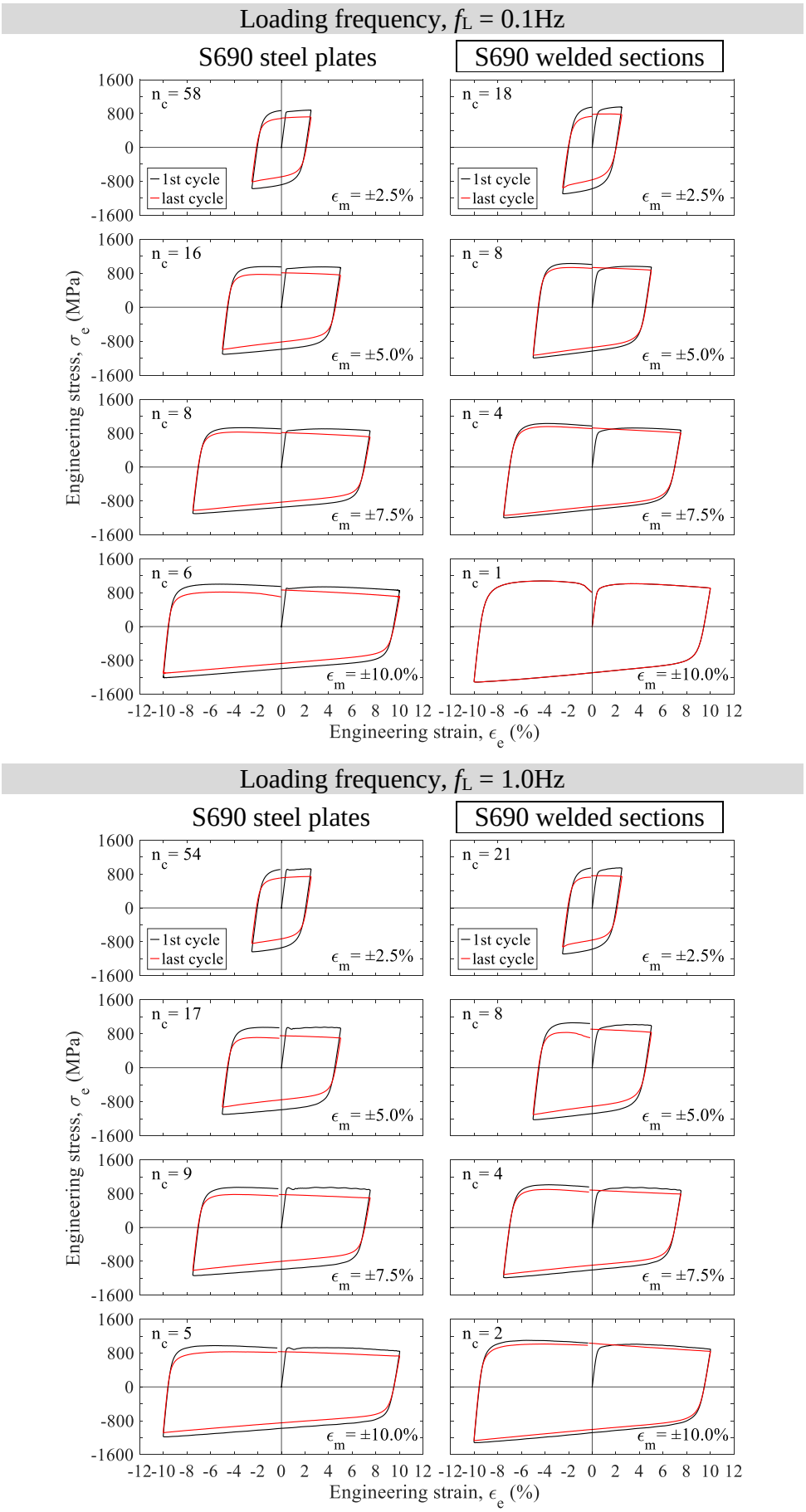

Figure 15 First and last cycles under Cyclic Protocol CT

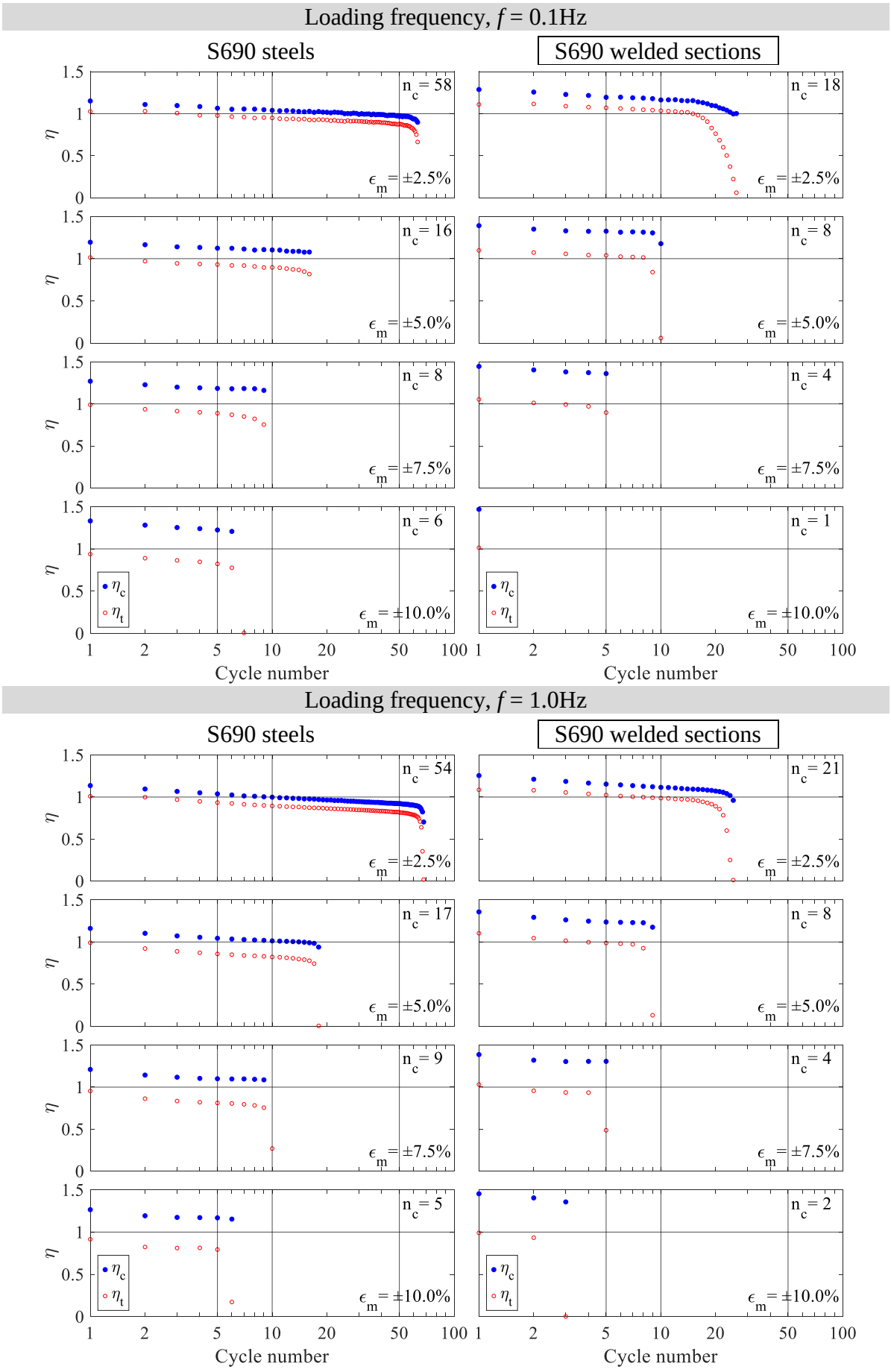

Figure 16 Strength modification factors against cycle numbers of S690 steels and welded sections

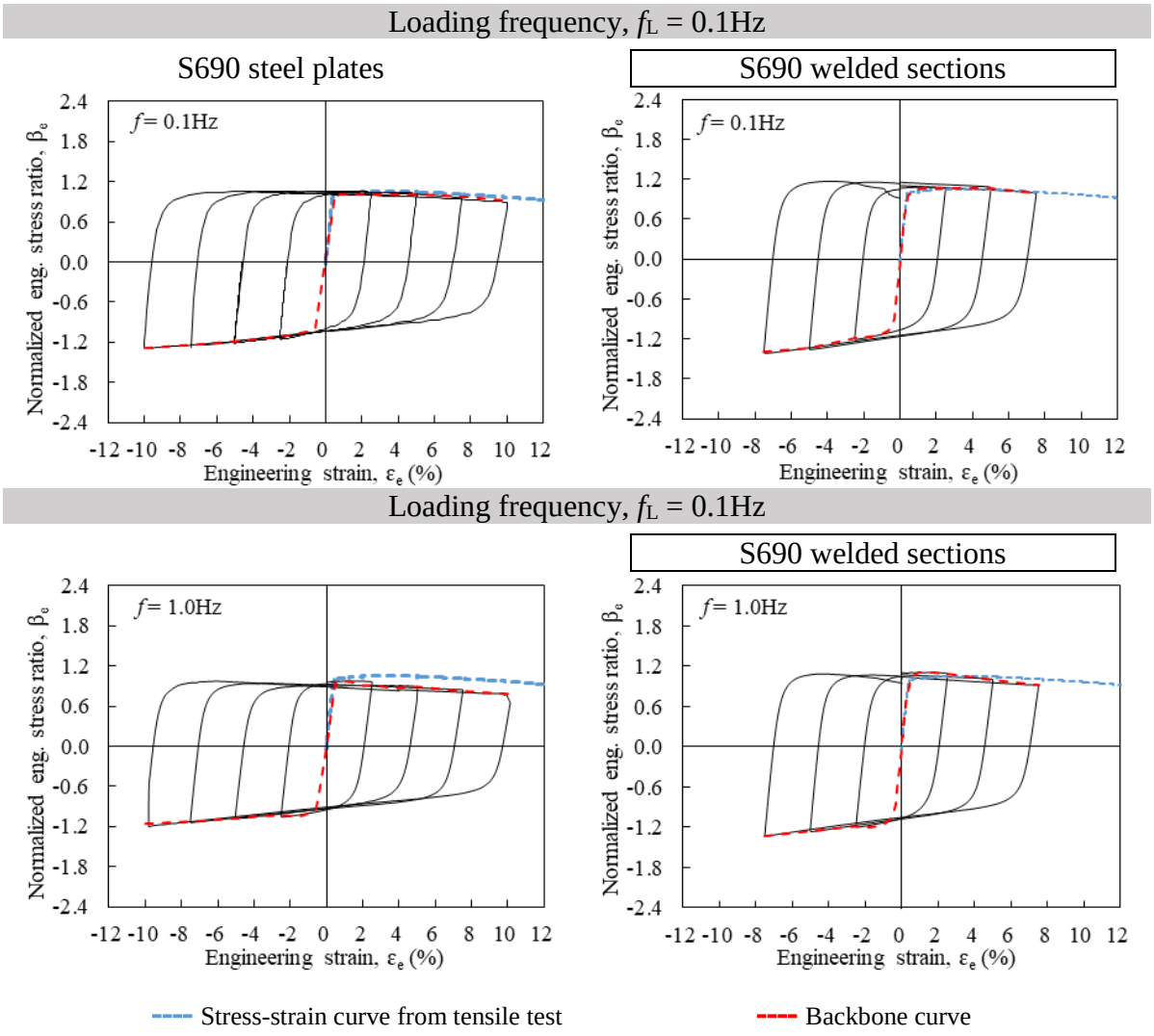

Figure 17 Hysteretic loops of both S690 steel plates and S690 welded sections under Cyclic Protocol NL

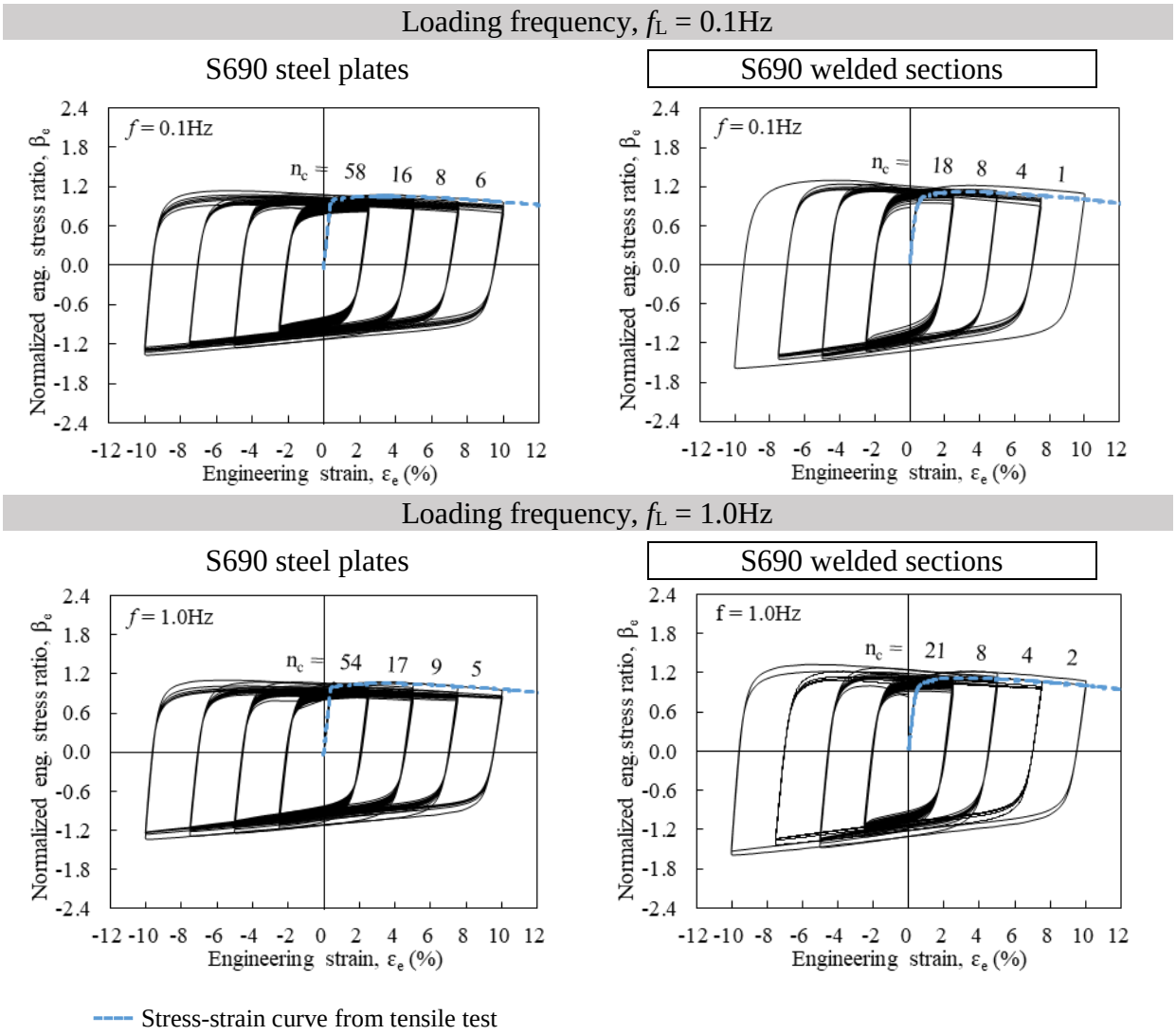

Figure 18 Hysteretic loops of both S690 steel plates and S690 welded sections under Cyclic Protocol CT

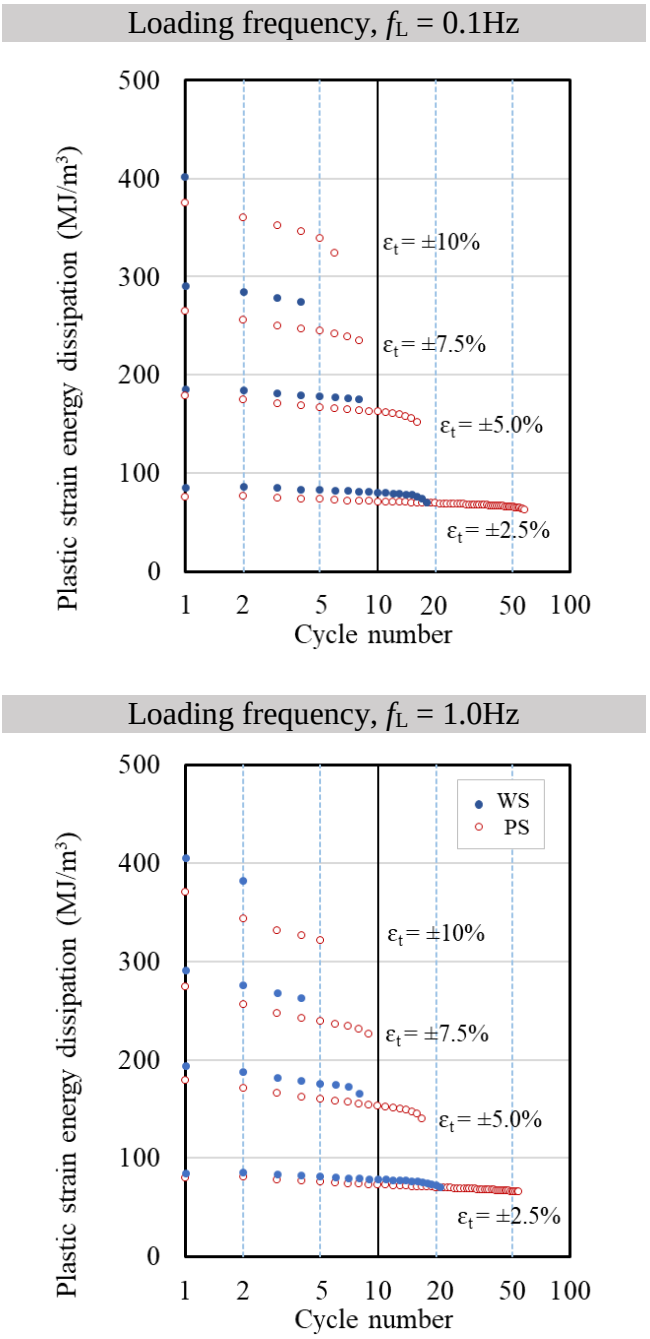

Figure 19 Energy dissipation performance of both S690 steel plates and S690 welded sections under Cyclic Protocol CT

Loading frequency, f_L = 0.1Hz

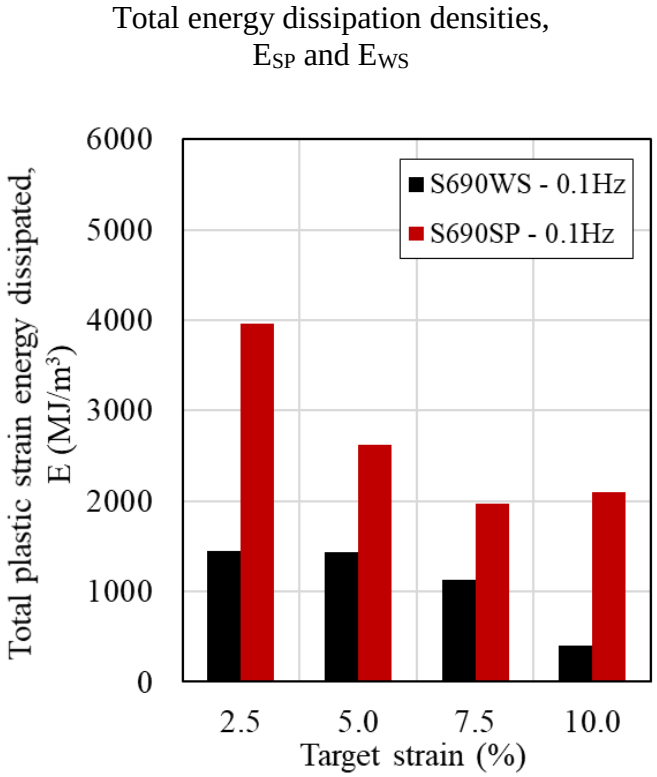

Loading frequency, f_L = 1.0Hz

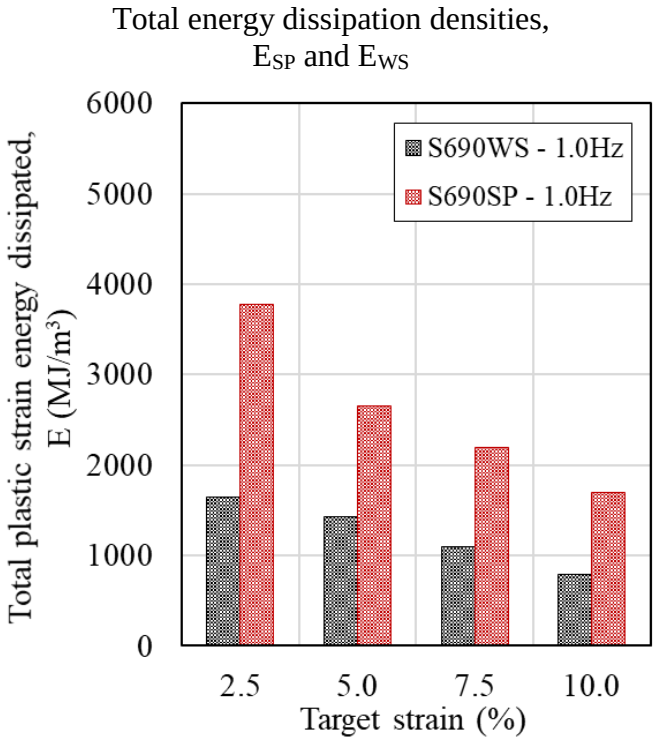

Figure 20 Energy dissipation densities of both S690 steel plates and S690 welded sections under Cyclic Protocol CT

Table 1 Materials specifications of S690 steels and the electrode

a) Chemical compositions (%) of S690 steels to EN 10025-6

Steels	C	Si	Mn	P	S	N	B	Cr	Cu	Mo	Nb	Ni	Ti	V	Jr
S690 to EN 10025-6	0.22	0.86	1.8	0.025	0.012	0.016	0.006	1.6	0.55	0.74	0.07	2.1	0.07	0.14	0.17

b) Chemical compositions (%) of the electrode

Electrode	C	Si	Mn	P	S	Ni	Cr	Mo	V
Lincoln 121K3C-H Plus	0.06 – 0.07	0.24- 0.29	1.56 – 1.88	0.010 – 0.011	0.007 – 0.012	2.21 – 2.25	0.04 – 0.07	0.53 – 0.65	0.00

Table 2 Welding parameters for S690 welded sections

S690 steels	Voltage (V)	Current (A)	Wire feeding speed (m per minute)	Welding speed (m/s)	Efficient ratio η	Heat input energy (kJ/mm)
10 mm thick plates	28.8 ~ 29.1	177 ~ 202	8.890	4.6	0.85	0.96 ~ 1.06 ±0.02

Table 3 Monotonic tensile tests on S690 steel plates and welded sections

a) Test programme

Coupon	Shape of coupons	Thickness of steel plates (mm)	Diameter d (mm)	Gauge length L_0 (mm)	Total length L (mm)
S690-T1 S690-T2	Funnel-shaped	16	5	10	184
S690H-T1 S690H-T2	Funnel-shaped	16	5	10	184

b) Mechanical properties

Coupon	Thickness of original plates (mm)	Young's modulus E (kN/mm^2)	Yield strength f_y (N/mm^2)	Tensile strength f_u (N/mm^2)	Elongation at fracture ε_L (%)	f_u/f_y
S690-T1	16	231.3	872	922	24.1	1.06
S690-T2		225.8	895	933	23.6	1.04
	Average	228.6	883	927	23.8	1.05
S690H-T1	16	202.8	833	936	19.1	1.12
S690H-T2		207.6	828	946	20.8	1.14
	Average	205.2	830	941	20.0	1.13

Table 4 Test programme of cyclic tests on S690 steel plates and welded sections

a) Funnel-shaped coupons of S690 steel plates – 10 mm thick

Diameter d (mm)	Gauge length L_0 (mm)	Cyclic protocol	Loading frequency f_L (Hz)	Target strain ε_T			
				±2.5%	±5.0%	±7.5%	±10.0%
5	10	NL	0.1	1	1	1	1
			1.0	1	1	1	1
		CT	0.1	1	1	1	1
			1.0	1	1	1	1

b) Funnel-shaped coupons of S690 welded sections – 10 mm thick

Diameter d (mm)	Gauge length L_0 (mm)	Cyclic protocol	Loading frequency f_L (Hz)	Target strain ε_T			
				±2.5%	±5.0%	±7.5%	±10.0%
5	10	NL	0.1	1	1	1	1
			1.0	1	1	1	1
		CT	0.1	1	1	1	1
			1.0	1	1	1	1

Table 5. Test results of cyclic tests on S690 steel plates and welded sections

Cyclic Protocol	Loading frequency f_L (Hz)	No. of cycles completed, n_c							
		±2.5%		±5.0%		±7.5%		±10.0%	
		Steel plates	Welded sections	Steel plates	Welded sections	Steel plates	Welded sections	Steel plates	Welded sections
NL	0.1	20	20	20	20	20	19	19	16
	1.0	20	20	20	20	20	20	19	17
CT	0.1	58	18	16	8	8	4	6	1
	1.0	54	21	17	8	9	4	5	2

Table 6. Strength modification factors at the first cycle of cyclic tests on S690 steel plates and welded sections under Cyclic Protocol CT

Strength modification factors	Loading frequency f_L (Hz)	Strength modification factors at the first cycle							
		±2.5%		±5.0%		±7.5%		±10.0%	
		Steel plates	Welded sections	Steel plates	Welded sections	Steel plates	Welded sections	Steel plates	Welded sections
η_t	0.1	1.03	1.11	1.01	1.10	0.99	1.05	0.94	1.01
η_c	0.1	1.15	1.29	1.19	1.39	1.27	1.45	1.33	1.47
η_t	1.0	1.01	1.09	0.99	1.10	0.95	1.03	0.91	0.99
η_c	1.0	1.14	1.26	1.16	1.36	1.21	1.39	1.26	1.45

Table 7. Total energy densities, E

Cyclic Protocol CT	Target strain, ε_T (%)	Total energy density, E (MJ/m^3)		E_{WS} / E_{SP}
		for steel plates E_{SP}	for welded sections E_{WS}	
Loading frequency, f_L = 0.1 Hz	±2.5	4,166	1,445	0.35
	±5.0	2,669	1,437	0.54
	±7.5	2,085	1,127	0.54
	±10.0	2,164	401	0.19
Loading frequency, f_L = 1.0 Hz	±2.5	3,852	1,642	0.43
	±5.0	2,692	1,428	0.53
	±7.5	2,271	1,097	0.48
	±10.0	1,749	786	0.45

Conflict of interests

The project leading to publication of this paper is partially funded by the Research Grants Council of the Government of Hong Kong SAR and the Research Committee of the Hong Kong Polytechnic University. Both technical and financial supports from the Chinese National Engineering Research Centre for Steel Construction (Hong Kong Branch) of the Hong Kong Polytechnic University are also gratefully acknowledged.